Fat body-derived cytokine Upd2 controls disciplined migration of tracheal stem cells in *Drosophila*

Pengzhen Dong[1,2], Yue Li[1,2], Yuying Wang[1,2], Qiang Zhao[1,2], Tianfeng Lu[6], Tianyu Guo[1,2], Jun Ma[7,8], Bing Yang[5,*], Honggang Wu[3,*], Hai Huang[1,2,4,*]

1 Department of Cell Biology, and Second Affiliated Hospital, Zhejiang University School of Medicine. Hangzhou, Zhejiang Province 310058.

2 State Key Laboratory of Transvascular Implantation Devices, Hangzhou 310009, China.

3 Zhejiang Key Laboratory of Precision Diagnosis and Therapy for Major Gynecological Diseases, Women's Hospital, Zhejiang University School of Medicine. Hangzhou, Zhejiang Province 310058.

4 Zhejiang Provincial Key Laboratory of Genetic & Developmental Disorders, Zhejiang University School of Medicine. Hangzhou 311121.

5 MOE Laboratory of Biosystem Homeostasis and Protection and Life Sciences Institute, Zhejiang University, Hangzhou, 310058, China.

6 Department of Developmental Biology & Neuroscience, Washington University in St. Louis, Missouri, United States, 63108.

7 Center for Genetic Medicine, the Fourth Affiliated Hospital, Zhejiang University School of Medicine, Hangzhou, Zhejiang 310058, China.

8 Institute of Genetics, Zhejiang University International School of Medicine, Hangzhou, Zhejiang 310058, China.

*Correspondence: bingyang@zju.edu.cn; honggangwu@zju.edu.cn; haihuang@zju.edu.cn

Abstract

Coordinated activation and directional migration of adult stem cells are essential for maintaining tissue homeostasis. *Drosophila* tracheal progenitors are adult stem cells that migrate posteriorly along the dorsal trunk to replenish degenerating branches that disperse the FGF mitogen. However, it is currently unknown how the overall anterior-to-posterior directionality of such migration is controlled. Here we show that individual progenitor cells migrate together in a concerted, disciplined manner, a behavior that is dependent on the neighboring fat body. We identify the fat body-derived cytokine, Upd2, in targeting and inducing JAK/STAT signaling in tracheal progenitors to maintain their directional migration. Perturbation of either Upd2 production in fat body or JAK/STAT signaling in trachea causes aberrant bidirectional migration of tracheal progenitors. We show that JAK/STAT signaling promotes the expression of genes involved in planar cell polarity leading to asymmetric localization of Fat in progenitor cells. We provide evidence that Upd2 transport requires Rab5- and Rab7-mediated endocytic sorting and Lbm-dependent vesicle trafficking. Our study thus uncovers an inter-organ communication in the control of disciplined migration of tracheal progenitor cells, a process that requires vesicular trafficking of fat body-derived cytokine Upd2 and JAK/STAT signaling-mediated activation of PCP genes.

Introduction

Adult stem cells are multipotent cell populations which inhabit their niche but mobilize to initiate tissue reconstruction during organismal growth and regeneration. An intriguing feature of stem cells is their capability of migrating in a disciplined directionality towards locations undergoing reconstruction (L. Li & Clevers, 2010). Such a highly disciplined movement is critical for maintaining tissue homeostasis and is influenced by various niche-intrinsic signals and external stimuli, and its aberrancy causes diseases such as hypertrophy (Zhou et al., 2024). The damaged tissue or distant organs that elicit systemic signals promote the migration of adult stem cells (Jones & Wagers, 2008). In addition, interactions with other cell types, soluble factors (e.g. cytokines, growth factors, and hormones) and tissue stiffness collectively bolster the mobilization of stem cells (Fuchs & Blau, 2020). Despite growing appreciation of adult stem cells as a primary source for tissue regeneration, the mechanism governing directional stem cell migration remains yet to be elucidated.

Drosophila tracheal progenitors are a population of adult stem cells that rebuild the degenerating trachea during metamorphosis. The progenitor cells reside in Tr4 and Tr5 metameres and start to move along the tracheal branch towards sites of regeneration (Pitsouli & Perrimon, 2010). Movement of these progenitor cells follows a stereotypical anterior-to-posterior axis (Figure 1A), thus representing a suitable system to investigate mechanisms controlling the directionality of stem cell migration. The activation of tracheal progenitors is stimulated by the morphogen Branchless (Bnl), fly homolog of fibroblast growth factor (FGF) (F. Chen & Krasnow, 2014), and the insulin hormone (Y. Li et al., 2022). Intercellular communication and synergy between organs also contribute to the branching morphogenesis (Perochon et al., 2021; Schottenfeld, Song, & Ghabrial, 2010; Tamamouna et al., 2021). The functional role of the interactions between trachea and other organs in modulating tracheal progenitor behavior has been largely unknown.

Drosophila fat body is the functional analog of mammalian adipose tissue and the major organ sensing various hormonal and nutritional signals to orchestrate systemic growth, metabolism and stem cell maintenance (Sriskanthadevan-Pirahas et al., 2022).

Fat body produces regulatory molecules known as fat body signals (FBSs), which remotely affect the activity of other organs (Ingaramo, Sanchez, Perrimon, & Dekanty, 2020; Zheng, Yang, & Xi, 2016). For instance, the fat body-to-brain signals modulate insulin-like peptides production (Rajan & Perrimon, 2012), visual attention and sleep behavior (Ertekin, Kirszenblat, Faville, & van Swinderen, 2020).

The *Drosophila* family of interleukin-6 (IL-6)-like cytokines consist of Unpaired (Upd, also called Outstretched), Upd2 and Upd3, and serve as mediators of systemic signaling. Whereas Upd1 and Upd3 derive from fly brain and plasmatocytes (Beshel, Dubnau, & Zhong, 2017; Woodcock et al., 2015), Upd2 is primarily produced by the fat body (Rajan, Housden, Wirtz-Peitz, Holderbaum, & Perrimon, 2017), although muscle-derived Upd2 is also reported (X. Zhao & Karpac, 2017). The Upd proteins act as ligands which bind to a common GP130-like receptor, Domeless (Dome) on target cells (Agaisse, Petersen, Boutros, Mathey-Prevot, & Perrimon, 2003; H. W. Chen et al., 2002). Upon association of ligands, the Dome receptors dimerize and recruit the non-receptor tyrosine kinase JAKs leading to their subsequent transactivation via phosphorylation. The transactivated JAKs then phosphorylate the tyrosine residues of their substrates, including the bound receptors and cytosolic STATs. The phosphorylation of STATs promotes their dimerization and nuclear translocation to activate transcriptional program (Darnell, 1997). JAK/STAT signaling requires the IL-6 cytokines (Heinrich et al., 2003), and is implicated in numerous cellular events including cell proliferation, differentiation, migration and apoptosis (O'Shea, Gadina, & Schreiber, 2002).

Here, we investigate molecular basis underlying directional stem cell migration using the *Drosophila* tracheal progenitors as a model. Our results identify a cytokine-mediated inter-organ communication between fat body and the progenitor cells that is necessary for their disciplined, directional migration. The directional migration of the progenitors relies on JAK/STAT signaling and its downstream targets of planar cell polarity (PCP) components. Importantly, the Upd2 cytokines derived from fat body are transported through vesicular trafficking to induce JAK/STAT signaling in tracheal progenitors. Our study reveals that tracheal progenitors establish migratory

directionality as they exit their niches and that the disciplined migration of the progenitors depends on an inter-organ signaling originating from the fat body.

112 **Results**

113 Dependence of tracheal progenitors on fat body

114 The fly tracheal progenitors are activated and move posteriorly along the dorsal trunk
115 (DT) at the onset of pupariation (Figure 1A). We set out to delve into the underlying
116 mechanisms of directional progenitor cell movement and tentatively surveyed organs
117 that may coordinate this process. In *Drosophila*, fat body resides anatomically in
118 proximity with trachea (Figure 1B, C; Video 1) and is the principal reservoir for
119 energy consumption. To determine whether the integrity of fat body is required for
120 tracheal progenitors, we perturbed larval or pupal fat body by expressing pro-
121 apoptotic cell death genes, *hid* and *reaper* (*rpr*), under the control of a fat body-
122 specific driver, *lsp2*-Gal4. Expression of *hid* and *rpr* in L3 stage impaired fat body
123 integrity and adipocyte abundance, and generated slender larvae and pupae (Figure 1-
124 figure supplement 1A-D). In these animals, the tracheal progenitors exhibited a sign
125 of undisciplined migration and tended to move bidirectionally (Figure 1D-F),
126 although their migration rate and proliferation remained unchanged (Figure 1-figure
127 supplement 1E-H). The undisciplined bidirectional migration behavior of tracheal
128 progenitors in fat body-defective animals is in stark contrast to control animals where
129 the progenitors migrated unambiguously towards posterior (Figure 1D-D" and Video
130 2). To gain a quantitative view of progenitor cell migration, we traced the movement
131 of individual cells by time-lapse confocal imaging. At 2hr APF, tracheal progenitors
132 from fat body deficit animals displayed a symmetrical distribution relative to the
133 junction between dorsal trunk (DT) and transverse connective (TC), compared with an
134 L-shape localization of niche-associated and migratory progenitors established by a
135 posterior movement in control (Figure 1G-H'). Gauging the vector denoting the
136 movement of each progenitor (Figure 1I-I') revealed that the traces of individual
137 progenitors in fat body-depleted animals exhibited a fan-shaped pattern (Figure 1J-J').
138 Owing to this undisciplined movement, entropy of the system was notably elevated
139 upon increased inconsistency of migration vectors (Figure 1K). The bidirectional
140 migratory progenitors displayed longer territory as assessed by binarized direction
141 (Figure 1L). Collectively, these results suggest that fat body has an integral role in

142 maintaining the discipline of tracheal progenitor movement.

143

144 Upd2-JAK/STAT signaling between fat body and trachea

145 Since fat body impacts the behavior of tracheal progenitors, we next attempted to
146 investigate the signal between these two interdependent organs. For this purpose, we
147 first performed RNA sequencing (RNA-seq) analysis of tracheal progenitors from
148 aforementioned fat body defective flies. The results revealed a dramatical alteration of
149 transcriptional program in tracheal progenitors upon the perturbation of fat body
150 (Figure 2-figure supplement 1A, B). Interestingly, the functional cluster of 'cytokine
151 activity' showed prominent enrichment in the differentially expressed genes (DEGs)
152 in progenitors from *lsp2>rpr.hid* pupae (Figure 2A). This raised the possibility that
153 certain cytokine-responsive signaling was induced in tracheal progenitors and the
154 signaling was compromised by impairment of fat body. Therefore, we proceeded to
155 analyze the expression of genes responsive to cytokine signaling. Analyzing the
156 RNA-seq data revealed that the cytokine-dependent JAK/STAT and Dpp signaling
157 were notably up-regulated upon the activation of progenitors (Figure 2B).
158 Importantly, fat body depletion led to suppression of target genes of JAK/STAT, PI3K
159 and Dpp signaling in tracheal progenitors, suggesting their dependence on the
160 function of fat body (Figure 2C).
161 To evaluate the roles of these cytokines and signaling proteins, we perturbed their
162 expression in fat body by the expression of RNAi constructs. Knockdown of various
163 cytokines specifically in fat body did not affect the direction of tracheal progenitor
164 migration (Figure 2-figure supplement 1C-J), except for *upd2*, whose depletion
165 phenocopied fat body ablation-induced bidirectional movement of tracheal
166 progenitors (Figure 2D-F and Video 3). These results suggest a role of fat body-
167 produced Upd2 in remotely regulating the tracheal progenitors.
168 Then, we performed surface proteome *in vivo* (J. Li et al., 2020) to investigate the
169 spectrum of molecules received by trachea (Figure 2-figure supplement 2). The
170 trachea-associated proteins were biotinylated through a reaction mediated by a
171 membrane-tethered horse radish peroxidase (HRP-CD2) (Figure 2-figure supplement

172 2A-D). Of the 1684 streptavidin-precipitated proteins captured by mass spectrometry
173 (Figure 2G), a functional cluster enriched for receptor signaling via JAK/STAT was
174 identified (Figure 2H). The JAK/STAT pathway is one of the principal cellular
175 signaling that responds to Upd2 ligand (Hombria, Brown, Hader, & Zeidler, 2005).
176 *Drosophila* JAK/STAT signaling is well-conserved (Arbouzova & Zeidler, 2006;
177 Zeidler, Bach, & Perrimon, 2000) and comprises a single JAK (Hopscotch, Hop) and
178 one STAT (Stat92E), in contrast to a handful of homologues (four JAK and seven
179 STAT genes) found in mammals. Domeless (Dome), the receptor for JAK/STAT
180 pathway, exhibited pronounced expression in the tracheal progenitors (Figure 2-figure
181 supplement 2E). To test if these Dome receptors actively interact with their ligands,
182 we adapted a technique to monitor ligand-receptor interaction *in vivo* (Michel, Raabe,
183 Kupinski, Perez-Palencia, & Bokel, 2011) and constructed a Dome variant (DIPF)
184 which only fluoresces in the ligand-binding and phosphorylated state (Figure 2I).
185 When expressed in the tracheal system, DIPF displayed robust fluorescent signal in
186 the tracheal progenitors (Figure 2J). These data suggest that receptor signaling of
187 JAK/STAT is active in the tracheal progenitors.
188 To analyze the functional importance of JAK/STAT signaling in tracheal progenitors,
189 we perturbed the principal components of this signaling, namely the receptor Dome,
190 signal transducer Hop or the downstream transcription factor Stat92E, by *btl*-Gal4-
191 driven expression of RNAi constructs. Under these conditions in which JAK/STAT
192 pathway is compromised, the tracheal progenitors aberrantly migrated anteriorly,
193 which is reminiscent of *upd2* loss-of-function in the fat body (Figure 3A-E and Video
194 4). In agreement with genetic perturbation of JAK/STAT signaling, pharmacological
195 inhibition of JAK by a small-molecule inhibitor, Tofacitinib (Palmroth et al., 2021),
196 also triggered bidirectional movement of tracheal progenitors (Figure 3F-H).
197 Concurrently, the activity of JAK/STAT pathway, as assessed by the Stat92E-GFP
198 reporter (Bach et al., 2007), was substantially impaired when components of the
199 pathway were depleted (Figure 3I-L, Q). Analysis of *upd*-Gal4 activity and the
200 transcription of *upd2* in various tissues indicates that Upd2 was primarily produced in
201 fat body and gut of the larvae (Figure 2-figure supplement 2F-H). To determine

202 whether the tracheal JAK/STAT signaling depends on fat body-derived Upd2, we
203 depleted Upd2 in fat body and observed that Stat92E-GFP signal in tracheal
204 progenitors was severely decreased, suggesting that JAK/STAT signaling in the
205 trachea requires fat body-produced Upd2 (Figure 3M-N, Q). Consistently, inhibition
206 of JAK/STAT signaling using Tofacitinib reduced the expression of Stat92E-GFP
207 (Figure 3O-Q). Taken together, these observations suggest that Upd2-responsive
208 JAK/STAT signaling in the trachea is essential for the disciplined migration of
209 progenitors.
210
211 Genes regulated by JAK/STAT signaling in the trachea
212 To gain a comprehensive understanding of the molecular details underlying the
213 discipline of tracheal progenitor migration, we conducted genomic chromatin
214 immunoprecipitation (ChIP-seq) to identify loci bound by Stat92E which functions as
215 the transcription factor of JAK/STAT pathway. This revealed a total of 21312 Stat92E
216 binding peaks, ~95.7% of which located within 2 kb of transcription start sites (TSSs)
217 of annotated genes (Figure 4-figure supplement 1A). In particular, 86% of the peaks
218 (18328 peaks) were enriched either in promoter regions or within gene bodies, and
219 66.1% of the peaks (13490 peaks) resided near the 5′ ends of annotated genes, namely
220 in the promoter regions, first exons and first introns (Figure 4-figure supplement 1B,
221 C). GO analysis of putative target genes of Stat92E identified one cluster associated
222 with establishment of planar polarity (Figure 4A). In line with this, the functional
223 class associated with establishment of planar polarity was also abundantly represented
224 among the differentially expressed genes (DEGs) upon the activation of tracheal
225 progenitors in larval-pupal transition (Figure 4B). Notably, Stat92E binding was
226 detected in the promoters and intronic regions of genes functioning in distal-to-
227 proximal signaling (Cho & Irvine, 2004), such as *dachsous* (*ds*), *four-jointed* (*fj*), *fz*,
228 *stan*, *Vang* and *fat2* (Figure 4C). Additionally, Stat92E occupied in the promoter
229 regions of *crb* and *yurt,* two genes involved in apical-basal polarity and tracheal tube
230 growth (Laprise et al., 2006; Schottenfeld-Roames & Ghabrial, 2012; Schottenfeld-
231 Roames, Rosa, & Ghabrial, 2014) (Figure 4-figure supplement 1D). The enrichment

232 of Stat92E in the promoters and/or regulatory regions of these putative targets was
233 confirmed by ChIP-qPCR (Figure 4-figure supplement 1E).
234 To further validate these putative Stat92E targets and investigate their dependence on
235 JAK/STAT signaling, we analyzed their expression from several fosmid transgenes
236 which have a GFP tag fused to *ds*, *fj* or *ft* and express at endogenous levels. Ds and Fj
237 were abundant in the progenitor cells, but were vastly reduced upon depletion of
238 *dome*, *hop* or *stat92E*, suggesting that they are regulated by JAK/STAT pathway
239 (Figure 4D-M). Furthermore, it is reported that the function of Ft is influenced by
240 cell-autonomous increase of Ds level and its protein level is enhanced by Ds reduction
241 (Ambegaonkar, Pan, Mani, Feng, & Irvine, 2012; Matakatsu & Blair, 2004), which is
242 also evidenced by our analysis using *dsRNAi* and *UAS-ds* in the tracheal progenitors
243 (Figure 4-figure supplement 2). In accordance with this notion, the level of Ft, as
244 assayed by the Ft-GFP reporter, was elevated by the reduction of JAK/STAT signaling
245 (Figure 4N-R). We also analyzed GFP-tagged fosmid transgenes of *fat2, crb* and *yurt*
246 and found that they were discernably reduced upon impairment of JAK/STAT
247 signaling, suggesting that they are also regulated by JAK/STAT pathway (Figure 4-
248 figure supplement 1F-T). Additionally, the transcription of *ds*, *fj*, *ft*, *fat2*, *crb*, and *yurt*
249 was compromised by expression of *stat92ERNAi* (Figure 4-figure supplement 1U). In
250 sum, these results suggest that JAK/STAT promotes components involved in the
251 establishment of polarity in tracheal cells.
252
253 <u>The roles of JAK/STAT targets in the disciplined migration</u>
254 To evaluate the functional roles of the polarity proteins in tracheal progenitor
255 migration, we perturbed their expression in the tracheal progenitors by expressing
256 RNAi against *ds*, *ft* or *fj*, which were identified by ChIP-seq as the targets of
257 JAK/STAT. In these flies, tracheal progenitors exhibited bidirectional movement,
258 which is reminiscent of the impairment of JAK/STAT signaling (Figure 5A-E and
259 Video 5). Similar observations were obtained by over-expression of *ft* or *ds* in the
260 trachea (Figure 5-figure supplement 1A-D), consistent with previous reports that both
261 loss- and gain-of-function of PCP components disrupt the planar cell polarity (Adler,

262 Taylor, & Charlton, 2000; Tree et al., 2002; Vinson & Adler, 1987). The disciplined
263 migration of tracheal progenitors was also impaired by the expression of *fat2RNAi*,
264 *crbRNAi*, *yurtRNAi* or *scbRNAi* (Figure 5-figure supplement 1E-I).
265 Migratory cells generate protrusions at the leading edge to initiate movement (Cetera
266 et al., 2014). The normal posteriorly migrating tracheal progenitors extend protrusions
267 towards the migratory directions (Figure 5-figure supplement 2A), but in the
268 bidirectionally moving progenitors in which Upd2 in fat body was perturbed,
269 extensive filopodia were projected from both the anterior and posterior fronts (Figure
270 5-figure supplement 2B, C), indicating that the aberrantly anteriorly moving
271 progenitors may adopt the identity as those moving posteriorly. Bidirectionally
272 migrating progenitors induced by perturbation of JAK/STAT signaling did not alter
273 the expression of the tracheal inducer, *branchless* (*bnl*) (Figure 5-figure supplement
274 2D, E). Further analysis revealed that the progenitors exhibited elevated levels of Ft at
275 the leading edge where they attached to dorsal trunk (DT) (Figure 5F-G).
276 Accordingly, progenitors that underwent bidirectional movement exhibited
277 pronounced abundance of Ft at both the anterior and posterior frontal edges (Figure
278 5H-J). To further evaluate the functional roles of Ft-Ds-Fj module in disciplined
279 migration, we utilized the high-mobility carcinoma cells, SKOV-3, and found that
280 perturbation of Fj that phosphorylates the extracellular cadherin domains of both Ft
281 and Ds and modifies their heterophilic binding (Thomas & Strutt, 2012), Ft or Ds
282 concurrently displayed compromised directionality and reduced consistency of
283 movement in a two-dimensional culture (Figure 5K-M and Figure 5-figure
284 supplement 3). Together with the results in previous sections, these observations
285 suggest that the activated tracheal progenitors establish a disciplined migration
286 through the asymmetrical distribution of polarity proteins which is directed by an
287 Upd2-JAK/STAT signaling stemming from the remote organ of fat body.
288
289 <u>Upd2 in the fat body-produced vesicle</u>
290 Besides the JAK/STAT signaling, another functional class enriched for vesicle-
291 mediated transport was prominent from our surface proteome analysis of the trachea

292 (Figure 2H). A series of components that function in vesicle trafficking were
293 identified. It has been reported that IL-6 cytokines tend to be encapsulated in
294 secretory vesicles (Kandere-Grzybowska et al., 2003; Verboogen, Ter Beest,
295 Honigmann, & van den Bogaart, 2018). To visualize Upd2 production and investigate
296 its transportation kinetics, an upd2-mCherry transgene was developed and expressed
297 under the control of *lsp2*-Gal4, which enabled tracking the dynamics of Upd2 in fat
298 body (Figure 6A). In agreement with Upd2 being transported through vesicles,
299 administration of L3 larvae with Brefeldin A (BFA), which pharmacologically inhibits
300 vesicle formation and transport, sequestered Upd2 proteins in fat body (Figure 6B, C).
301 To track the destination of the Upd2-containing vesicles, we examined mCherry
302 signals in adjacent tissues and detected considerable amount of Upd2 puncta in the
303 tracheal progenitors (Figure 6D). BFA treatment reduced Upd2-mCherry puncta in the
304 tracheal progenitors, suggesting that tracheal progenitors receive vesicular Upd2 from
305 the fat body (Figure 6E, F). Perturbation of Grasp65, a Golgi reassembly stacking
306 protein previously implicated in Upd2 secretion (Rajan et al., 2017), also led to
307 sequestration of Upd2-containing vesicles in fat body (Figure 6G, H, J). The vesicle
308 formation, function and extracellular movement are dependent on the tetraspanin
309 superfamily proteins (Andreu & Yanez-Mo, 2014). We surveyed all the tetraspanin
310 orthologs in fly for potential roles in Upd2 vesicle formation and transport. When
311 expressing *lbmRNAi* in fat body, Upd2-containing vesicles were vastly increased
312 (Figure 6I, J). Meanwhile, perturbation of vesicle secretion or transport by expressing
313 *grasp65RNAi* or *lbmRNAi* in fat body eliminated the presence of fat body-origin Upd2
314 in the trachea, suggesting that fat body-produced Upd2-containing vesicles function
315 cell non-autonomously and contribute to other tissues/organs (Figure 6K-N). It should
316 be noted that knockdown of *upd2* in the trachea did not alter the discipline of tracheal
317 progenitor migration (Figure 2-figure supplement 1K-M). Collectively, these results
318 suggest that fat body-produced Upd2 undergoes vesicle-mediated trafficking.
319
320 <u>The vesicular transport in JAK/STAT signaling</u>
321 The results in previous section suggest that the ligand of JAK/STAT signaling is

322 transported in a manner that depends on vesicle trafficking. To validate the role of fat
323 body-produced vesicles in inter-organ signaling, we used genetic and pharmacological
324 tools to perturb different processes of vesicle trafficking in fat body and monitored
325 JAK/STAT signaling in the tracheal progenitors. Expression of *grasp65RNAi* in fat
326 body reduced the activity of JAK/STAT signaling in the trachea, as assessed by the
327 Stat92E-GFP reporter (Figure 7A, B). Similarly, RNAi targeting expression of *lbm* in
328 fat body vanished JAK/STAT signal transduction in the trachea (Figure 7C). Rab
329 GTPases coordinate vesicle trafficking and production (Stenmark, 2009) and have
330 been shown to play pivotal roles in the regulation of intracellular trafficking of FGFR
331 and EGFR (Letizia, Espinas, Giannios, & Llimargas, 2023; Olivares-Castineira &
332 Llimargas, 2017), and were identified in the surface proteome analysis. Consistently,
333 knockdown of *rab5* or *rab7* in fat body reduced the activity of JAK/STAT signaling in
334 the progenitor cells (Figure 7D-F). Corroborating the genetic manipulations, BFA
335 treatment that impeded vesicular transport also resulted in impairment of JAK/STAT
336 signaling in trachea (Figure 7G-I). Taking advantage of the aforementioned DIPF
337 reporter to assess the response of receiving cells to ligands, we found that the
338 fluorescent signal of DIPF was compromised upon the presence of BFA, but was
339 unaffected by inhibitors that target the downstream JAK protein (Figure 7J-M),
340 suggesting that signaling ligands are less abundant in the recipient progenitor cells
341 and that the vesicle-mediated transport of ligands is essential for JAK/STAT signaling.
342 Phenotypically, the tracheal progenitors exhibited bidirectional migration in BFA-
343 treated flies, which phenocopies JAK/STAT loss-of-function (Figure 7N-P). In
344 concord with this observation, depletion of *grasp65* or *lbm* also led to bidirectional
345 movement (Figure 7Q-S'', and Video 6). Similar observations were made in tracheal
346 progenitors with either *rab5* or *rab7* knockdown (Figure 7T-V), whereas perturbation
347 of neither *rab2* nor *rab3* affected the disciplined progenitor migration (Figure 7-figure
348 supplement 1A-F). Taken together, these results suggest that JAK/STAT signaling in
349 the trachea is dependent on the vesicle-mediated transport of its ligands from fat body.
350

351 <u>The interaction between Upd2 and endocytic machinery</u>

352 Our results described thus far suggest that Upd2 emanating from fat body signals to
353 JAK/STAT signaling in the trachea. To further explore the molecular basis underlying
354 the vesicular transport of Upd2, we monitored Rab5-GFP and Rab7-GFP in fat body,
355 which mark early and late endosomes, respectively (Vonderheit & Helenius, 2005).
356 The fat body-produced Upd2 appeared vesicular (Figure 8A) and both Rab5 and Rab7
357 were found adjacent to the Upd2-harboring vesicles, suggesting that both Rab
358 GTPases function in the transport of Upd2 (Figure 8A'-B''). In contrast, Rab3
359 exhibited non-overlapping distribution with Upd2 (Figure 7-figure supplement 1G-
360 G''). Furthermore, we observed that Grasp65 was in close proximity to Upd2-
361 containing vesicles, indicating its integral roles in these vesicles (Figure 8C-C''). In
362 addition, Upd2 was observed to colocalize with the tetraspanin, Lbm (Figure 8D-D'').
363 At higher resolution, Upd2 and Lbm showed close association in a supramolecular
364 configuration (Figure 8D'''and 8D''''), corroborating its role in the transport of Upd2.
365 To determine if Upd2 interacts with the coordinators of vesicle trafficking, we
366 employed the Duolink in situ proximity ligation assay (PLA) which revealed strong
367 interactions between Upd2 and Rabs, such as Rab5 and Rab7 (Figure 8E-H), as well
368 as Lbm (Fig 8I, J). The interaction was further validated by the revelation that Upd2
369 co-immunoprecipitated with Rab5 and Rab7 (Figure 8K, L). The presence of Upd2 in
370 Lbm-containing vesicles was also evidenced in S2 cells (Figure 8-figure supplement
371 1A-C'') and co-IP experiment showed that Lbm physically associated with Upd2 in
372 both fat body and S2 cells (Figure 8M and Figure 8-figure supplement 1D). To further
373 understand the biogenesis of Lbm-containing vesicles that transport Upd2, we
374 generated an Lbm chimera tagged with a pH-sensitive GFP variant, pHluorin
375 (Yoshihara, Adolfsen, Galle, & Littleton, 2005). PHluorin fluorescence is squelched at
376 the low pH domain such as in intravesicular compartments, but becomes detectable
377 when exposed to the extracellular environment, thus enabling detection of exocytosis
378 and endocytosis. Fat body expressing Lbm-pHluorin produced GFP puncta at the
379 plasma membrane (Figure 8N), and the GFP signal was also detected in the trachea,
380 suggesting the reception and internalization of Lbm-containing vesicles by tracheal
381 cells (Figure 8O). However, the GFP fluorescence in both fat body and trachea was

382 dramatically decreased by BFA treatment, suggesting that Lbm-containing vesicles
383 are diminished (Figure 8-figure supplement 1E-H). Accordingly, the signals of Lbm-
384 pHluorin in both fat body and responding tracheoblasts were apparently compromised
385 when Rab5 or Rab7 was perturbed (Figure 8P-S), suggesting that the biogenesis and
386 production of Lbm-containing vesicles depend on Rab-mediated vesicle trafficking.
387 Taken together, these results suggest that fat body-derived Upd2 interacts with Rab-
388 mediated endocytic trafficking system to control the disciplined movement of tracheal
389 progenitors.
390

Discussion

Resident stem cells and progenitors are mobilized to regenerate damaged or degenerated tissue. Despite the large distance between the niche where stem cells interact with their microenvironments and the destination for reconstruction, their commitment to a stereotyped track implicates sophisticated mechanism that controls disciplined migration as stem cells are activated and move out of the niche. While primary inducers expressed by damaged tissues are in play to coordinate the newly generated architecture with the degenerated counterpart (F. Chen & Krasnow, 2014), the present study elucidates an integral role of Upd2-JAK-STAT pathway in regulating the expression of polarity-related genes and maintaining the disciplined migration of tracheal progenitors (Figure 8T). The transport of Upd2 from fat body to trachea suggests intensive inter-organ communication during the migration of tracheal progenitors.

Several possibilities could account for the JAK/STAT-dependent polarity. The signaling components of JAK/STAT pathway could exhibit polarized localization (Sotillos, Diaz-Meco, Moscat, & Castelli-Gair Hombria, 2008). Alternatively, this signaling may activate genes controlling cell polarity and adhesion (Mallart et al., 2024; Tsurumi et al., 2011). Functional interplay between JAK/STAT signaling and cell polarity has been observed in various contexts (Chatterjee et al., 2023; Zeidler, Perrimon, & Strutt, 1999). Our results support a role of JAK/STAT signaling in promoting expression of genes with established roles in planar polarity, which may hallmark the route for the migration of the tracheal progenitor cells. Epithelial cells exhibit two aspects of polarity: apical-basal polarity and planar cell polarity (PCP). The latter refers to the collective alignment of cell polarity within the plane of an epithelial sheet (Zallen, 2007). Molecularly, PCP is generated by the asymmetry of a group of proteins (PCP proteins) that mediate communication between neighboring cells (Barlan, Cetera, & Horne-Badovinac, 2017; Matis & Axelrod, 2013; Williams, Donoughe, Munro, & Horne-Badovinac, 2022). In *Drosophila*, the components of PCP are considered to group functionally into two core modules. The seven-pass transmembrane protein Frizzled (Fz), the cytosolic proteins Dishevelled (Dsh), Diego

421 (Dgo), the four-pass transmembrane protein Strabismus (Stbm, also known as Van
422 Gogh (Vang)) and the cytosolic protein Prickle (Pk) belong to the first module. The
423 second module consists of Fat (Ft; also known as cadherin-related tumor suppressor),
424 Dachsous (Ds), Four-jointed (Fj) and Atro (a transcription repressor) (Peng &
425 Axelrod, 2012). Intensive functional interplay occurs between these two modules
426 (Ayukawa et al., 2014). Aberrant activity of the core PCP proteins leads to
427 misoriented hairs and complex swirling patterns (D. Ma, Yang, McNeill, Simon, &
428 Axelrod, 2003; Wong & Adler, 1993). In addition to arrangement of epithelial
429 appendages, PCP pathway is also required for collective and directed cell movements
430 (Munoz-Soriano, Belacortu, & Paricio, 2012). The migratory cell cohort is polarized
431 into 'pioneer' cells that lead the trailing followers (Vitorino & Meyer, 2008).
432 Our data indicate that expression of Ds, Fj, Fz, Stan and Fat2, core components or
433 regulators of PCP, depends on JAK/STAT pathway. The interaction between atypical
434 cadherin Fat (Ft) and its ligand, Dachsous (Ds) directs core protein asymmetry (Strutt
435 & Strutt, 2021; Yang, Axelrod, & Simon, 2002). Phenotypically, aberrancy of PCP
436 protein abundance, either excessive core protein or deficit in expression gradients,
437 gives rise to similar morphological abnormality (Adler et al., 2000; Casal, Struhl, &
438 Lawrence, 2002; Taylor, Abramova, Charlton, & Adler, 1998; Tree et al., 2002).
439 Consistent with this notion, gain-of-function of Fj or Ds phenocopies that of
440 perturbation of PCP proteins. JAK/STAT signaling promotes the expression of Ds, but
441 reduces Ft expression (Figure 4). Thereby, perturbation of JAK/STAT signaling
442 disrupts the Ds-Ft system.
443 A precedent for JAK/STAT signaling in directional cell movement is border cell
444 migration from anterior to posterior compartment during *Drosophila* oogenesis.
445 Migration of the border cells is guided by a gradient of PDGF and VEGF chemokines
446 (Duchek, Somogyi, Jekely, Beccari, & Rorth, 2001). Loss of either *hop* (encoding
447 JAK) or *stat* in the border cells impinges their recruitment into the cluster and
448 subsequent migration (Silver, Geisbrecht, & Montell, 2005). Our results suggest that
449 JAK/STAT signaling does not serve as a guidance cue for tracheal progenitors, but
450 rather directs the directionality of cell movement. The downstream PCP components

451 may contribute to either polarity of progenitors or cell-cell interactions between the
452 progenitors and tracheal cells that they track along. It remains unknown how
453 individual progenitor cells perceive directional information and convert it into group
454 choreography.
455 We identified the fly fat body as the major source for the JAK/STAT signaling ligand,
456 Upd2 production. Fat body is functionally equivalent to the mammalian liver which
457 stores proteins, lipids and sugars and functions as an energy reservoir (S. Li, Yu, &
458 Feng, 2019). It supplies proteins and/or hormones that are utilized by other organs,
459 and thereby serves as an interchange center to disperse systemic hormonal and
460 nutritional signals. For instance, it generates collagen IV to decorate imaginal discs
461 and produces xanthine dehydrogenase for eye pigmentation (Pastor-Pareja & Xu,
462 2011; Reaume, Clark, & Chovnick, 1989). The transport between fat body and trachea
463 has been reported on a secreted chitin deacetylase, Serpentine (Serp), which is
464 expressed by fat body and contributes to tracheal morphogenesis (Dong, Miao, &
465 Hayashi, 2014). Our results reveal that fat body also signals to regulate the disciplined
466 migration of tracheal progenitors through the dispersion of Upd2 cytokines. These
467 studies collectively suggest that fat body orchestrates systemic tissue growth and
468 patterning and that metabolic regulation is critical for adult stem cells.
469 Proteins that are locally produced can execute systemic function in distant organs. A
470 possible route of transport is through the hemolymph or bloodstream and taken up by
471 the target tissues. The signaling proteins such as cytokines can be packaged in
472 extracellular vesicles with various dimensions (Buzas, 2023; Javeed et al., 2021). A
473 precedent of vesicular transport of signaling molecules is reported in migrasomes
474 whose diameter exceeds 500 nm (Jiang et al., 2019).
475 These extracellular vesicles mediate cell-to-cell communication (Colombo, Raposo, &
476 Thery, 2014), perhaps at a distance (Hood, San, & Wickline, 2011) and even traverse
477 between organs (Corrigan et al., 2014). The vesicular Upd2 is able to signal at
478 recipient cells, suggesting that the activity of Upd2 is preserved in the vesicle, and it
479 is released upon vesicle fusion. Compared with conventional extracellular vesicles
480 such as exosomes, the Upd2-containing vesicles possess larger dimension. Its

481 production and trafficking depend on GRASP-mediated unconventional secretion and
482 interaction with Lbm. Lbm belongs to the tetraspanin protein family that contains four
483 transmembrane domains. The mammalian homologs of tetraspanins, CD9, CD63,
484 CD81 or CD37 are principal constituents of extracellular vesicles. The Lbm-
485 containing vesicles are regulated by GRASP-mediated secretion and are sensitive to
486 pharmacological inhibition of EV transport.
487 It has been proposed that tetraspanins facilitate regeneration and wound healing in
488 cultural cells and single-cell plasma membrane. Tetraspanin-enriched macrodomains
489 are assembled into a ring-like structure (Huang, Zhang, Wang, & Yu, 2022), which is
490 recruited to large membrane wounds and promotes membrane repair (Wang et al.,
491 2022). The present study adds another dimension to the roles of tetraspanin proteins in
492 tissue regeneration which can be ascribed to transport of signaling proteins and
493 modulation of stem cells.
494
495

Materials and methods

Key Resources Table

REAGENT or RESOURCE	SOURCE	IDENTIFIER
Antibodies		
Rabbit anti-GFP (1:400)	Invitrogen	#A11122
Mouse anti-GFP (1:1000)	Abclonal	#AE012
Mouse anti-mCherry (1:1000)	Abclonal	#AE002
Rabbit anti-tubulin (1:5000)	Baoke	#BK7010
Phalloidin Alexa Fluor 640 (1:50)	Biotum	#00050
HRP-conjugated Streptavidin (1:5000)	Proteintech	#SA00001-0
Alexa Fluor 488 (1:200)	Abclonal	#AS053
Alexa Fluor 555 (1:200)	Abclonal	#AS007
DAPI	VECTASHIELD	#H1200
Reagents		
Halocarbon oil 700	Sigma	#H8898
RNeasy Micro Kit	QIAGEN	#74004
SMART-Seq v4 Ultra low input RNA Kit	Takara	#634889
AMPure XP	Beckman Coulter	#A63882
TruePrep DNA Library Prep Kit V2	Vazyme	#TD501
Anti-FLAG M2 Magnetic Beads	Millipore	#8823
BXXP	APEXBIO	#A8012
Experimental models: Organisms/strains		
D. melanogaster:*UAS-upd2RNAi*	Tsinghua Stock Center	THU1331
D. melanogaster:*UAS-domeRNAi*	Tsinghua Stock Center	THU0574
D. melanogaster:*UAS-hopRNAi*	Tsinghua Stock Center	THU5762
D. melanogaster:UAS-stat92ERNAi	Tsinghua Stock Center	THU0573
D. melanogaster:*UAS-lbmRNAi*	Tsinghua Stock Center	THU2602
D. melanogaster:*UAS-grasp65RNAi*	Tsinghua Stock Center	TH04282.N
D. melanogaster:*UAS-rab5RNAi*	Tsinghua Stock Center	TH02192.N
D. melanogaster:*UAS-rab7RNAi*	Tsinghua Stock Center	TH02539.N
D. melanogaster:UAS-fjRNAi	Tsinghua Stock Center	THU201500988.S
D. melanogaster:*UAS-fat2RNAi*	Tsinghua Stock Center	THU4120
D. melanogaster:*UAS-yurtRNAi*	Tsinghua Stock Center	THU1740
D. melanogaster:UAS-crbRNAi	Tsinghua Stock Center	THU2783
D. melanogaster:UAS-scbRNAi	Tsinghua Stock Center	THU3905
D. melanogaster:*10XStat92E-GFP*	Tsinghua Stock Center	THJ0273
D. melanogaster:*Stat92E-GFP*	BDSC	#38670
D. melanogaster:*UAS-grasp65-GFP*	BDSC	#8507
D. melanogaster:*Ds::GFP*	BDSC	#59425
D. melanogaster:*Yurt::GFP*	VDRC	#318067
D. melanogaster:*Crb::GFP*	VDRC	#318384
D. melanogaster:*Ft::GFP*	VDRC	#318477
D. melanogaster:*Fj::GFP*	VDRC	#318457
D. melanogaster:*UAS-dsRNAi*	VDRC	#36219
D. melanogaster:*UAS-ftRNAi*	VDRC	#9396
D. melanogaster:*UAS-ft*	From Dr. Xianjue Ma	N/A
D. melanogaster:*UAS-ds*	From Dr. Xing Wang	N/A
D. melanogaster:*UAS-fat2-GFP*	From Dr. Shunfan Wu	N/A
D. melanogaster:*UAS-GFP-Rab7*	From Dr. Xiaohang Yang	N/A
D. melanogaster:*UAS-GFP-Rab5*	From Dr. Xiaohang Yang	N/A

Oligonucleotides		
Primer α-tubulin84b Forward:CACACCACCCTGGAGCATTC	This paper	N/A
Primer α-tubulin84b Reverse:CCAATCAGACGGTTCAGGTTG	This paper	N/A
Primer upd2 Forward:TCAATCCGTATCGCGGTCTG	This paper	N/A
Primer upd2 Reverse:AGAAGAGTCGCAGGTTGTGG	This paper	N/A
Primer ds Forward:ACAACCGAACTCGAACCGAA	This paper	N/A
Primer ds Reverse:AGTAGCATCACACACAAGTGA	This paper	N/A
Primer ft Forward:CTGGATCGAGAGCAGCAGAG	This paper	N/A
Primer ft Reverse:GACGGTAAATTCTCGCGCAC	This paper	N/A
Primer fj Forward:ATTACTCAAGCGGTTGGGGG	This paper	N/A
Primer fj Reverse:CGGTTCCTGTTCCTGTCTCC	This paper	N/A
Primer fat2 Forward:TATCTGCGCCCATACGCATT	This paper	N/A
Primer fat2 Reverse:TCTCATCGGCCTTGCTTTGT	This paper	N/A
Primer yurt Forward:GGTCAGCTCAGGGTGACTATC	This paper	N/A
Primer yurt Reverse:ATTGGTAAGCTTGGCGTTGC	This paper	N/A
Primer crb Forward:CAGCAGTGTTTGAACGGTGG	This paper	N/A
Primer crb Reverse:AGGCAGTGACCAATGGGG	This paper	N/A
Software and algorithms		
Fiji / ImageJ	NIH	RRID:SCR_002285
GraphPad Prism 8.0	GraphPad Software	https://www.graphpad.com/scientific-software/prism/
Zen 3.1	Zeiss	https://www.zeiss.com.cn/corporate/home.html
PCA-flow	Bradski, G.[79]	https://www.drdobbs.com/open-source/the-opencv-library
Deposited data		
Raw and processing Data	This paper	GSE256177 https://www.iprox.cn/page/PSV023.html;?url=1708323921277ZyfCqvupguyijvyndyf

502 **Fly lines and husbandry**

503 All flies were reared on normal cornmeal and agar medium at 25°C unless noted.
504 UAS-upd2RNAi (THU1331), UAS-domeRNAi (THU0574), UAS-hopRNAi
505 (THU5762), UAS-stat92ERNAi (THU0573), UAS-lbmRNAi (THU2602), UAS-
506 grasp65RNAi (TH04282.N), UAS-rab5RNAi (TH02192.N), UAS-rab7RNAi
507 (TH02539.N), UAS-fjRNAi (THU201500988.S), UAS-fat2RNAi (THU4120), UAS-
508 yurtRNAi (THU1740), UAS-crbRNAi (THU2783) and UAS-scbRNAi (THU3905)
509 were ordered from Tsinghua Stock Center. Stat92E-GFP (BSDC#38670), UAS-
510 grasp65-GFP (BSDC#8507), Ds::GFP (BSDC#59425) were from Bloomington
511 Drosophila Stock Center. Yurt::GFP (v318067), Crb::GFP (v318384), Ft::GFP
512 (v318477), Fj::GFP (v318457), UAS-dsRNAi (v36219), and UAS-ftRNAi (v9396)
513 were obtained from VDRC. UAS-ft was kindly provided by Dr. Xianjue Ma, UAS-ds
514 was kindly provided by Dr. Xing Wang and UAS-fat2-GFP was from Dr. Shunfan
515 Wu. UAS-GFP-rab5 and UAS-GFP-rab7 were kindly provided by Dr. Xiaohang
516 Yang.

517 **Plasmid construction and transgenic flies**

518 To generate UAS-upd2-mCherry and UAS-lbm-GFP transgenic flies, the coding
519 sequence of upd2 or lbm was PCR amplified from a fly cDNA library and cloned into
520 a pUAST vector with C-terminal mCherry or GFP.

521 The DIPF reporter was generated by first fusing cpYFP and *Drosophila* FKBP12 and
522 subsequently ligating to the dome cDNA via a GTG linker. The above product was
523 then cloned into a pUAST vector and verified by DNA sequencing, and injected into
524 y[1] M{vasint.Dm}ZH-2A w[*]; P{CaryP}attP2 recipient flies or *w1118* following
525 standard *Drosophila* transformation injection procedures (Core Facility of Drosophila
526 Resource and Technology, SIBCB, CAS).

527 **Cell culture and transfection**

528 S2 cells were grown in Schneider Drosophila Medium (Gibco, #21720024)

529 supplemented with 10% (v/v) Fetal Bovine Serum (FBS, Gibco) and 1% (v/v)
530 Penicillin Streptomycin (Pen/Strep, Life Technologies) at 28°C with 0.2% CO_2.
531 Transfection was conducted with 5 μg plasmids (act-GAL4, UAS-lbm-GFP, UAS-
532 upd2-mCherry) using Effectene Transfection Reagent (QIAGEN, #301425).

533 **Quantitative reverse transcription PCR**

534 Larval or pupal trachea were dissected in cold PBS, and then transferred to RNA
535 extraction reagent (AG21101). Next, reverse transcription was performed using qPCR
536 RT Mix with gDNA Remover reagent (AG11706). qPCR was performed using the
537 Universal SYBR Select Master Mix (AG11701) with a Bio-Rad system. The
538 foldchange of target gene expression was normalized to that of α-tubulin. The primers
539 are listed in Key Resources Table.

540 **Western Blotting and Co-immunoprecipitation**

541 Total protein was extracted from cells or tissues by RIPA buffer supplemented with a
542 protease inhibitor cocktail (Merck, #11836170001) and phenylmethanesulfonyl
543 fluoride (Beyotime, #ST507), separated by 10% SDS-PAGE gels and transferred to
544 PVDF membrane (Millipore, #IPVH00010). Blots were detected with an ECL
545 Western Blotting detection system (Bio-Rad). For co-immunoprecipitation, lysates of
546 larval fat body or transfected S2 cells were incubated overnight at 4°C with protein A
547 Magnetic beads (Thermo Scientific, #2736141) pre-coated with GFP antibody
548 (Invitrogen, #A11122). Immunoprecipitates were eluted in SDS-containing loading
549 buffer for subsequent immunoblotting analysis. Antibodies for immunoblotting
550 include: α-tubulin (Baoke, #BK7010), α-HRP-conjugated Streptavidin (Proteintech,
551 #SA00001-0), α-GFP (Abclonal, #AE012, 1:1000); α-mCherry (Abclonal, #AE002,
552 1:1000).

553 **Proximity Ligation Assay**

554 Proximity ligation assay (PLA) was carried out with Duolink® In Situ Detection
555 Reagents Far Red (Sigma Aldrich, #DUO92013) according to manufacturer's

556 instructions, using the probes anti-rabbit PLUS (Sigma Aldrich, #DUO92002) and
557 anti-mouse MINUS (Sigma Aldrich, #DUO92004). Briefly, larval fat body was
558 dissected and fixed in 4% formaldehyde. After permeabilization, the samples were
559 incubated with primary antibodies overnight at 4°C. Then, the samples were washed
560 with PLA buffer A, hybridized with PLA probes, ligated, and amplified. Samples were
561 washed twice with PLA buffer B (Sigma Aldrich, #DUO82049) and fluorescence
562 images were taken with an LSM Zeiss 900 inverted confocal laser scanner
563 microscope.

564 **Immunofluorescence**

565 Trachea from white pupae (0hr APF) were dissected in PBS and fixed with 4%
566 formaldehyde for 25 min at room temperature. After washes, trachea samples were
567 permeabilized with 1% TritonX-100 in PBS, and then blocked in 10% goat serum.
568 Incubation with primary antibody (GFP, 1:400; lacZ, 1:40) was performed at 4°C with
569 gentle rotation for overnight. Then, the samples were incubated with secondary
570 antibodies conjugated to Alexa Fluor 488 or 555 (1:200) and Phalloidin (1:50) for 2
571 hrs. After washing, samples were mounted in antifade mounting medium with DAPI
572 (VECTASHIELD) and imaged under an LSM Zeiss 900 inverted confocal laser
573 scanner microscope.

574 **Live imaging of pupal trachea stem cells**

575 White pupae (0hr APF) were briefly washed in double distilled water and mounted in
576 halocarbon oil 700 (Sigma, #H8898). The pupae were positioned with forceps to bring
577 a single dorsal trunk of the trachea up for optimal imaging of Tr4 and Tr5 metameres.
578 Then, pupae were immobilized by a 22x30 mm No.1.5 high precision coverslip
579 spaced by vacuum grease. Time-lapse images were captured by an LSM Zeiss 900
580 inverted confocal laser scanner microscope.

581 **RNA sequencing of tracheal progenitors**

582 Total RNA was isolated from the Tr4 and Tr5 metamere progenitors dissected from

583 1hr APF pupae using RNeasy Micro Kit (QIAGEN, #74004). SMART-Seq v4 Ultra
584 low input RNA Kit (Takara, #634889) was used for first-strand and second-strand
585 cDNA synthesis and double-stranded cDNA end repair. Double-stranded cDNAs were
586 cleaned using AMPure XP (Beckman Coulter, #A63882). Then cDNAs were
587 subjected to tagmentation and ligation to adaptors to generate the sequencing libraries
588 using TruePrep DNA Library Prep Kit V2 for Illumina kit (Vazyme, #TD501). The
589 quality and concentration of the libraries were assessed using the Agilent High
590 Sensitivity DNA Kit and Bioanalyzer 2100 (Agilent Technologies) and submitted to
591 150 bp paired-end high throughput sequencing using Hiseq4000 (Illumina).

592 Analysis of RNA-seq data was performed using a computer system equipped with
593 multiple processors. Clean reads were mapped to the *Drosophila* genome sequence
594 using Hisat2 with default parameters. Successfully mapped reads were counted using
595 FeatureCounts. Differential gene expression analysis was performed using the
596 DESeq2 package. Adjusted p-value < 0.05 was used as the threshold to identify the
597 differentially expressed genes. Gene ontology and KEGG pathway enrichment
598 analyses for the differentially expressed genes were conducted using the Database for
599 Annotation, Visualization and Integrated Discovery (DAVID).

600 **Chromatin Immunoprecipitation**

601 Third instar larval trachea from Stat92E-Flag (BDSC, #38670) were fixed in 1%
602 formaldehyde. The fixation reaction was terminated by adding glycine (125 mM).
603 Trachea were washed and resuspended in lysis buffer, and sonicated to generate 200-
604 600 bp DNA fragments. Procedures of immunoprecipitation and ChIP sequencing
605 library construction were as previously described (Y. Li et al., 2022). Anti-FLAG M2
606 Magnetic Beads (Millipore, #8823) were used for enriched DNA binding to
607 transcription factor Stat92E.

608 Immunoprecipitated DNA was subjected to next-generation sequencing using the
609 Epicenter Nextera DNA Sample Preparation Kit or to real-time PCR. Library
610 construction was performed using the High Molecular Weight tagmentation buffer

611 (source), and tagmented DNA was linearly amplified by PCR. The libraries were then
612 sequenced on a Novaseq according to manufacturer's standard protocols. The
613 sequences were processed using *Fastqc* and low-quality bases and adaptor
614 contamination were trimmed by *cutadapt*. Filtered reads were mapped to *Drosophila*
615 genome using *BWA mem* algorithm. Peaks were called using macs2 *callpeak* (Q. Zhao
616 et al., 2019) and plotted using pyGenomeTracks. GO analysis of biological processes
617 was conducted by DAVID.

618 **Cell-surface proteomics of fly trachea**

619 Trachea from white pupae were dissected in pre-cooled Schneider Medium (Gibco)
620 and collected in 1.5 mL low-binding tube (Axygen) containing 500 μL Schneider
621 Medium. The samples were washed with 500 μL fresh medium and incubated with
622 100 μM BXXP (APEXBIO, #A8012) for 1 hr on ice with occasional pipetting.
623 Labeling reaction was initiated by adding 1 mM (0.03%) H_2O_2 to the sample-
624 containing medium and proceeded for 7 minutes at room temperature. The reaction
625 was immediately quenched by five thorough washes with PBS containing 10 mM
626 sodium ascorbate (Aladdin, #S105024) and 5 mM Trolox (APEXBIO, #C3183). For
627 biochemical characterization or proteomic sample preparation, the quenching solution
628 was drained, and the trachea in minimal residual quenching solution were quickly
629 frozen in liquid nitrogen and stored at 80°C. LC-MS/MS analysis was performed
630 using a Q Exactive HF-X instrument (Thermo Fisher) coupled with Easy-nLC 1200
631 system. The acquired MS raw data were processed using MaxQuant version 2.0.1.0
632 (Max Planck Institute of Biochemistry, Germany). Label-free quantification (LFQ)
633 was set with a default parameter and iBAQ was selected.

634 **Optic Flow Analysis**

635 <u>Motion Correlation</u>

636 Time-lapse images of trachea progenitor cells were captured every 5 minutes over a
637 total duration of 2 hrs using an LSM Zeiss 900 microscope. The movies and images

were subjected to a three-step motion collection using ImageJ (Schneider, Rasband, & Eliceiri, 2012) as follows:

(1) Images were transformed to grey scale.

(2) Automated stabilization was performed on grey images by image stabilizer.

(3) The feature points were mapped and affine transformation was applied using big warp (Bogovic, Hanslovsky, Wong, & Saalfeld, 2015).

Optical flow

Optical flow represents the pattern of motion of pixels in a sequence of images. Between two consecutive frames $I(x, y, t)$ and $I(x, y, t + \Delta t)$, the optical flow vector $\mathbf{v} = (v_x, v_y)$ represents the motion of pixels during this time. The optical flow constraint equation is shown below:

$$I_x v_x + I_y v_y + I_t = 0$$

We adopted the PCA-flow algorithm (Bradski, 2000) in openCV library (cv::optflow::OpticalFlowPCAFlow) in which the sparse optical flow vectors within each small region of the image sequence are calculated before training optical flow fields via principal component analysis (PCA) (Wulff & Black, 2015). The vectors were assembled to generate a smooth vector field of optic flow using the learning linear models of flow. The PCA-flow was validated for the efficiency and robustness.

Variance in 1D axis

We developed a robust estimator to evaluate the variance of optic flow projection along the 1D migration axis between samples. The vector length is normalized by a frame-specific normalization factor κ to fit with scale of optic flow computed among different frames.

$$\kappa = Q_{0.9}\{||v||_2 \mid v \in vectorfield\}$$

where Q is the quantile function. The variance is computed as $\mathrm{Var}(\{||v||_2 > Q_{0.2} \mid v \in vectorfield\})$ and scaled to 0-1 by $\mathrm{Var}(x)/\big(\mathrm{Var}(x) + \mathrm{Var}(y)\big)$.

Random Variable

The direction of optic flow in each volume was assigned to ’left’ or ’right’. Then the distribution of the binarized directions is modeled as a Bernoulli random variable $\mathrm{X} \sim \mathrm{Bernoulli(p)}$ with PMF

$$P(X = x) = \begin{cases} p & \text{if } x = 1, \\ 1 - p & \text{if } x = 0. \end{cases}$$

Binary Entropy

The entropy for Bernoulli random variable $\mathrm{X} \sim \mathrm{Bernoulli(p)}$ is defined as

$$H_{binary}(X) = -p\log(p) - (1-p)log(1-p)$$

The entropy evaluates the information contained in the random variable (also called uncertainty). In this case, when $p = 0.5$, it reaches the maxima 1; if the variable is determinate (i.e. p=0 or 1), the entropy is zero. More directed cell migration leads to a lower entropy in optic flow since the certainty is high for the migration direction. We estimated p by computing ratio of left and right direction

$$p = \frac{\#left}{\#left + \#right}$$

Image and statistical analysis

Confocal z-stack images were analyzed to extract information of fluorescent intensity and number of particles using ImageJ. All statistical analysis was conducted using GraphPad Prism 8.0. Mean and standard error of the mean (SEM) were shown. Unpaired t-tests with Benjamin’s correction were used to evaluate statistical significance between groups.

Acknowledgements

We thank Drs Thomas Kornberg, David Strutt, Xiaohang Yang, Markus Affolter, Mark Krasnow, Stefan Luschnig, Kai Yuan, Xing Wang, Zhouhua Li, Xianjue Ma, Sarah Bray, Yiming Zheng and Shunfan Wu for generously providing reagents; Core Facility of Drosophila Resource and Technology, SIBCB, CAS for injection service; Bloomington Drosophila Stock Center, Kyoto Stock Center, Vienna stock center, Tsinghua Stock Center for fly stocks; Developmental Studies Hybridoma Bank for antibodies; all members of Huang lab and Kornberg lab for discussions and constructive suggestions. This work has been financially supported by NSFC92168101, NSFC32070784 and Thousand Young Talent Program to H.H., NSFC32000574 to H.G.W., National Key R&D Program of China (2022YFF0608402) and Chinese National Natural Science Funds (22374128) to B.Y. and NSFC32300699, LQ24C120001 and Postdoctoral Fellowship Foundation 2023M733098 to Y.L..

Author contributions

Conceptualization: H.H., P.Z.D.; Methodology: B.Y., P.Z.D., T.F.L., T.Y.G; Investigation: P.Z.D., Y.L., Y.Y.W., Q.Z., T.F.L., H.G.W; Supervision: J.M., H.H., H.G.W, B.Y.; Writing: J.M., H.H., P.Z.D, H.G.W.

Declaration of interests

The authors declare no competing interests.

References

Adler, P. N., Taylor, J., & Charlton, J. (2000). The domineering non-autonomy of frizzled and van Gogh clones in the Drosophila wing is a consequence of a disruption in local signaling. *Mech Dev, 96*(2), 197-207. doi:10.1016/s0925-4773(00)00392-0

Agaisse, H., Petersen, U. M., Boutros, M., Mathey-Prevot, B., & Perrimon, N. (2003). Signaling role of hemocytes in Drosophila JAK/STAT-dependent response to septic injury. *Dev Cell, 5*(3), 441-450. doi:10.1016/s1534-5807(03)00244-2

Ambegaonkar, A. A., Pan, G., Mani, M., Feng, Y., & Irvine, K. D. (2012). Propagation of Dachsous-Fat planar cell polarity. *Curr Biol, 22*(14), 1302-1308. doi:10.1016/j.cub.2012.05.049

Andreu, Z., & Yanez-Mo, M. (2014). Tetraspanins in extracellular vesicle formation and function. *Front Immunol, 5*, 442. doi:10.3389/fimmu.2014.00442

Arbouzova, N. I., & Zeidler, M. P. (2006). JAK/STAT signalling in Drosophila: insights into conserved regulatory and cellular functions. *Development, 133*(14), 2605-2616. doi:10.1242/dev.02411

Ayukawa, T., Akiyama, M., Mummery-Widmer, J. L., Stoeger, T., Sasaki, J., Knoblich, J. A., . . . Yamazaki, M. (2014). Dachsous-dependent asymmetric localization of spiny-legs determines planar cell polarity orientation in Drosophila. *Cell Rep, 8*(2), 610-621. doi:10.1016/j.celrep.2014.06.009

Bach, E. A., Ekas, L. A., Ayala-Camargo, A., Flaherty, M. S., Lee, H., Perrimon, N., & Baeg, G. H. (2007). GFP reporters detect the activation of the Drosophila JAK/STAT pathway in vivo. *Gene Expr Patterns, 7*(3), 323-331. doi:10.1016/j.modgep.2006.08.003

Barlan, K., Cetera, M., & Horne-Badovinac, S. (2017). Fat2 and Lar Define a Basally Localized Planar Signaling System Controlling Collective Cell Migration. *Dev Cell, 40*(5), 467-477 e465. doi:10.1016/j.devcel.2017.02.003

Beshel, J., Dubnau, J., & Zhong, Y. (2017). A Leptin Analog Locally Produced in the Brain Acts via a Conserved Neural Circuit to Modulate Obesity-Linked Behaviors in Drosophila. *Cell Metab, 25*(1), 208-217. doi:10.1016/j.cmet.2016.12.013

Bogovic, J. A., Hanslovsky, P., Wong, A., & Saalfeld, S. (2015). Robust registration of calcium images by learned contrast synthesis. *2016 IEEE 13th International Symposium on Biomedical Imaging (ISBI)*, 1123-1126.

Bradski, G. (2000). The OpenCV library. *Dr Dobb's J. Software Tools, 25*, 120-125. Retrieved from https://cir.nii.ac.jp/crid/1570009750919616256

Buzas, E. I. (2023). The roles of extracellular vesicles in the immune system. *Nat Rev Immunol, 23*(4), 236-250. doi:10.1038/s41577-022-00763-8

Casal, J., Struhl, G., & Lawrence, P. A. (2002). Developmental compartments and planar polarity in Drosophila. *Curr Biol, 12*(14), 1189-1198. doi:10.1016/s0960-9822(02)00974-0

Cetera, M., Ramirez-San Juan, G. R., Oakes, P. W., Lewellyn, L., Fairchild, M. J., Tanentzapf, G., . . . Horne-Badovinac, S. (2014). Epithelial rotation promotes the global alignment of contractile actin bundles during Drosophila egg chamber elongation. *Nat Commun, 5*, 5511. doi:10.1038/ncomms6511

Chatterjee, D., Cong, F., Wang, X. F., Machado Costa, C. A., Huang, Y. C., & Deng, W. M. (2023). Cell polarity opposes Jak/STAT-mediated Escargot activation that drives intratumor heterogeneity in a Drosophila tumor model. *Cell Rep, 42*(2), 112061. doi:10.1016/j.celrep.2023.112061

Chen, F., & Krasnow, M. A. (2014). Progenitor outgrowth from the niche in Drosophila trachea is

guided by FGF from decaying branches. *Science, 343*(6167), 186-189. doi:10.1126/science.1241442

Chen, H. W., Chen, X., Oh, S. W., Marinissen, M. J., Gutkind, J. S., & Hou, S. X. (2002). mom identifies a receptor for the Drosophila JAK/STAT signal transduction pathway and encodes a protein distantly related to the mammalian cytokine receptor family. *Genes Dev, 16*(3), 388-398. doi:10.1101/gad.955202

Cho, E., & Irvine, K. D. (2004). Action of fat, four-jointed, dachsous and dachs in distal-to-proximal wing signaling. *Development, 131*(18), 4489-4500. doi:10.1242/dev.01315

Colombo, M., Raposo, G., & Thery, C. (2014). Biogenesis, secretion, and intercellular interactions of exosomes and other extracellular vesicles. *Annu Rev Cell Dev Biol, 30*, 255-289. doi:10.1146/annurev-cellbio-101512-122326

Corrigan, L., Redhai, S., Leiblich, A., Fan, S. J., Perera, S. M., Patel, R., . . . Wilson, C. (2014). BMP-regulated exosomes from Drosophila male reproductive glands reprogram female behavior. *J Cell Biol, 206*(5), 671-688. doi:10.1083/jcb.201401072

Darnell, J. E., Jr. (1997). STATs and gene regulation. *Science, 277*(5332), 1630-1635. doi:10.1126/science.277.5332.1630

Dong, B., Miao, G., & Hayashi, S. (2014). A fat body-derived apical extracellular matrix enzyme is transported to the tracheal lumen and is required for tube morphogenesis in Drosophila. *Development, 141*(21), 4104-4109. doi:10.1242/dev.109975

Duchek, P., Somogyi, K., Jekely, G., Beccari, S., & Rorth, P. (2001). Guidance of cell migration by the Drosophila PDGF/VEGF receptor. *Cell, 107*(1), 17-26. doi:10.1016/s0092-8674(01)00502-5

Ertekin, D., Kirszenblat, L., Faville, R., & van Swinderen, B. (2020). Down-regulation of a cytokine secreted from peripheral fat bodies improves visual attention while reducing sleep in Drosophila. *PLoS Biol, 18*(8), e3000548. doi:10.1371/journal.pbio.3000548

Fuchs, E., & Blau, H. M. (2020). Tissue Stem Cells: Architects of Their Niches. *Cell Stem Cell, 27*(4), 532-556. doi:10.1016/j.stem.2020.09.011

Heinrich, P. C., Behrmann, I., Haan, S., Hermanns, H. M., Muller-Newen, G., & Schaper, F. (2003). Principles of interleukin (IL)-6-type cytokine signalling and its regulation. *Biochem J, 374*(Pt 1), 1-20. doi:10.1042/BJ20030407

Hombria, J. C., Brown, S., Hader, S., & Zeidler, M. P. (2005). Characterisation of Upd2, a Drosophila JAK/STAT pathway ligand. *Dev Biol, 288*(2), 420-433. doi:10.1016/j.ydbio.2005.09.040

Hood, J. L., San, R. S., & Wickline, S. A. (2011). Exosomes released by melanoma cells prepare sentinel lymph nodes for tumor metastasis. *Cancer Res, 71*(11), 3792-3801. doi:10.1158/0008-5472.CAN-10-4455

Huang, Y., Zhang, X., Wang, H. W., & Yu, L. (2022). Assembly of Tetraspanin-enriched macrodomains contains membrane damage to facilitate repair. *Nat Cell Biol, 24*(6), 825-832. doi:10.1038/s41556-022-00920-0

Ingaramo, M. C., Sanchez, J. A., Perrimon, N., & Dekanty, A. (2020). Fat Body p53 Regulates Systemic Insulin Signaling and Autophagy under Nutrient Stress via Drosophila Upd2 Repression. *Cell Rep, 33*(4), 108321. doi:10.1016/j.celrep.2020.108321

Javeed, N., Her, T. K., Brown, M. R., Vanderboom, P., Rakshit, K., Egan, A. M., . . . Matveyenko, A. V. (2021). Pro-inflammatory beta cell small extracellular vesicles induce beta cell failure through activation of the CXCL10/CXCR3 axis in diabetes. *Cell Rep, 36*(8), 109613. doi:10.1016/j.celrep.2021.109613

Jiang, D., Jiang, Z., Lu, D., Wang, X., Liang, H., Zhang, J., . . . Yu, L. (2019). Migrasomes provide regional cues for organ morphogenesis during zebrafish gastrulation. *Nat Cell Biol, 21*(8), 966-977. doi:10.1038/s41556-019-0358-6

Jones, D. L., & Wagers, A. J. (2008). No place like home: anatomy and function of the stem cell niche. *Nat Rev Mol Cell Biol, 9*(1), 11-21. doi:10.1038/nrm2319

Kandere-Grzybowska, K., Letourneau, R., Kempuraj, D., Donelan, J., Poplawski, S., Boucher, W., . . . Theoharides, T. C. (2003). IL-1 induces vesicular secretion of IL-6 without degranulation from human mast cells. *J Immunol, 171*(9), 4830-4836. doi:10.4049/jimmunol.171.9.4830

Laprise, P., Beronja, S., Silva-Gagliardi, N. F., Pellikka, M., Jensen, A. M., McGlade, C. J., & Tepass, U. (2006). The FERM protein Yurt is a negative regulatory component of the Crumbs complex that controls epithelial polarity and apical membrane size. *Dev Cell, 11*(3), 363-374. doi:10.1016/j.devcel.2006.06.001

Letizia, A., Espinas, M. L., Giannios, P., & Llimargas, M. (2023). The TNFR Wengen regulates the FGF pathway by an unconventional mechanism. *Nat Commun, 14*(1), 5874. doi:10.1038/s41467-023-41549-3

Li, J., Han, S., Li, H., Udeshi, N. D., Svinkina, T., Mani, D. R., . . . Luo, L. (2020). Cell-Surface Proteomic Profiling in the Fly Brain Uncovers Wiring Regulators. *Cell, 180*(2), 373-386 e315. doi:10.1016/j.cell.2019.12.029

Li, L., & Clevers, H. (2010). Coexistence of quiescent and active adult stem cells in mammals. *Science, 327*(5965), 542-545. doi:10.1126/science.1180794

Li, S., Yu, X., & Feng, Q. (2019). Fat Body Biology in the Last Decade. *Annu Rev Entomol, 64*, 315-333. doi:10.1146/annurev-ento-011118-112007

Li, Y., Dong, P., Yang, Y., Guo, T., Zhao, Q., Miao, D., . . . Huang, H. (2022). Metabolic control of progenitor cell propagation during Drosophila tracheal remodeling. *Nat Commun, 13*(1), 2817. doi:10.1038/s41467-022-30492-4

Ma, D., Yang, C. H., McNeill, H., Simon, M. A., & Axelrod, J. D. (2003). Fidelity in planar cell polarity signalling. *Nature, 421*(6922), 543-547. doi:10.1038/nature01366

Ma, J., Chen, T., Wu, S., Yang, C., Bai, M., Shu, K., . . . Zhu, Y. (2019). iProX: an integrated proteome resource. *Nucleic Acids Research, 47*(D1), D1211-D1217. doi:10.1093/nar/gky869

Mallart, C., Netter, S., Chalvet, F., Claret, S., Guichet, A., Montagne, J., . . . Malartre, M. (2024). JAK-STAT-dependent contact between follicle cells and the oocyte controls Drosophila anterior-posterior polarity and germline development. *Nat Commun, 15*(1), 1627. doi:10.1038/s41467-024-45963-z

Matakatsu, H., & Blair, S. S. (2004). Interactions between Fat and Dachsous and the regulation of planar cell polarity in the wing. *Development, 131*(15), 3785-3794. doi:10.1242/dev.01254

Matis, M., & Axelrod, J. D. (2013). Regulation of PCP by the Fat signaling pathway. *Genes Dev, 27*(20), 2207-2220. doi:10.1101/gad.228098.113

Michel, M., Raabe, I., Kupinski, A. P., Perez-Palencia, R., & Bokel, C. (2011). Local BMP receptor activation at adherens junctions in the Drosophila germline stem cell niche. *Nat Commun, 2*, 415. doi:10.1038/ncomms1426

Munoz-Soriano, V., Belacortu, Y., & Paricio, N. (2012). Planar cell polarity signaling in collective cell movements during morphogenesis and disease. *Curr Genomics, 13*(8), 609-622. doi:10.2174/138920212803759721

O'Shea, J. J., Gadina, M., & Schreiber, R. D. (2002). Cytokine signaling in 2002: new surprises in the

Jak/Stat pathway. *Cell, 109 Suppl*, S121-131. doi:10.1016/s0092-8674(02)00701-8

Olivares-Castineira, I., & Llimargas, M. (2017). EGFR controls Drosophila tracheal tube elongation by intracellular trafficking regulation. *PLoS Genet, 13*(7), e1006882. doi:10.1371/journal.pgen.1006882

Palmroth, M., Kuuliala, K., Peltomaa, R., Virtanen, A., Kuuliala, A., Kurttila, A., . . . Isomaki, P. (2021). Tofacitinib Suppresses Several JAK-STAT Pathways in Rheumatoid Arthritis In Vivo and Baseline Signaling Profile Associates With Treatment Response. *Front Immunol, 12*, 738481. doi:10.3389/fimmu.2021.738481

Pastor-Pareja, J. C., & Xu, T. (2011). Shaping cells and organs in Drosophila by opposing roles of fat body-secreted Collagen IV and perlecan. *Dev Cell, 21*(2), 245-256. doi:10.1016/j.devcel.2011.06.026

Peng, Y., & Axelrod, J. D. (2012). Asymmetric protein localization in planar cell polarity: mechanisms, puzzles, and challenges. *Curr Top Dev Biol, 101*, 33-53. doi:10.1016/B978-0-12-394592-1.00002-8

Perochon, J., Yu, Y., Aughey, G. N., Medina, A. B., Southall, T. D., & Cordero, J. B. (2021). Dynamic adult tracheal plasticity drives stem cell adaptation to changes in intestinal homeostasis in Drosophila. *Nat Cell Biol, 23*(5), 485-496. doi:10.1038/s41556-021-00676-z

Pitsouli, C., & Perrimon, N. (2010). Embryonic multipotent progenitors remodel the Drosophila airways during metamorphosis. *Development, 137*(21), 3615-3624. doi:10.1242/dev.056408

Rajan, A., Housden, B. E., Wirtz-Peitz, F., Holderbaum, L., & Perrimon, N. (2017). A Mechanism Coupling Systemic Energy Sensing to Adipokine Secretion. *Dev Cell, 43*(1), 83-98 e86. doi:10.1016/j.devcel.2017.09.007

Rajan, A., & Perrimon, N. (2012). Drosophila cytokine unpaired 2 regulates physiological homeostasis by remotely controlling insulin secretion. *Cell, 151*(1), 123-137. doi:10.1016/j.cell.2012.08.019

Reaume, A. G., Clark, S. H., & Chovnick, A. (1989). Xanthine dehydrogenase is transported to the Drosophila eye. *Genetics, 123*(3), 503-509. doi:10.1093/genetics/123.3.503

Schneider, C. A., Rasband, W. S., & Eliceiri, K. W. (2012). NIH Image to ImageJ: 25 years of image analysis. *Nat Methods, 9*(7), 671-675. doi:10.1038/nmeth.2089

Schottenfeld-Roames, J., & Ghabrial, A. S. (2012). Whacked and Rab35 polarize dynein-motor-complex-dependent seamless tube growth. *Nat Cell Biol, 14*(4), 386-393. doi:10.1038/ncb2454

Schottenfeld-Roames, J., Rosa, J. B., & Ghabrial, A. S. (2014). Seamless tube shape is constrained by endocytosis-dependent regulation of active Moesin. *Curr Biol, 24*(15), 1756-1764. doi:10.1016/j.cub.2014.06.029

Schottenfeld, J., Song, Y., & Ghabrial, A. S. (2010). Tube continued: morphogenesis of the Drosophila tracheal system. *Curr Opin Cell Biol, 22*(5), 633-639. doi:10.1016/j.ceb.2010.07.016

Silver, D. L., Geisbrecht, E. R., & Montell, D. J. (2005). Requirement for JAK/STAT signaling throughout border cell migration in Drosophila. *Development, 132*(15), 3483-3492. doi:10.1242/dev.01910

Sotillos, S., Diaz-Meco, M. T., Moscat, J., & Castelli-Gair Hombria, J. (2008). Polarized subcellular localization of Jak/STAT components is required for efficient signaling. *Curr Biol, 18*(8), 624-629. doi:10.1016/j.cub.2008.03.055

Sriskanthadevan-Pirahas, S., Turingan, M. J., Chahal, J. S., Thorson, E., Khan, S., Tinwala, A. Q., &

Grewal, S. S. (2022). Adipose mitochondrial metabolism controls body growth by modulating systemic cytokine and insulin signaling. *Cell Rep, 39*(6), 110802. doi:10.1016/j.celrep.2022.110802

Stenmark, H. (2009). Rab GTPases as coordinators of vesicle traffic. *Nat Rev Mol Cell Biol, 10*(8), 513-525. doi:10.1038/nrm2728

Strutt, H., & Strutt, D. (2021). How do the Fat-Dachsous and core planar polarity pathways act together and independently to coordinate polarized cell behaviours? *Open Biol, 11*(2), 200356. doi:10.1098/rsob.200356

Tamamouna, V., Rahman, M. M., Petersson, M., Charalambous, I., Kux, K., Mainor, H., . . . Pitsouli, C. (2021). Remodelling of oxygen-transporting tracheoles drives intestinal regeneration and tumorigenesis in Drosophila. *Nat Cell Biol, 23*(5), 497-510. doi:10.1038/s41556-021-00674-1

Taylor, J., Abramova, N., Charlton, J., & Adler, P. N. (1998). Van Gogh: a new Drosophila tissue polarity gene. *Genetics, 150*(1), 199-210. doi:10.1093/genetics/150.1.199

Thomas, C., & Strutt, D. (2012). The roles of the cadherins Fat and Dachsous in planar polarity specification in Drosophila. *Dev Dyn, 241*(1), 27-39. doi:10.1002/dvdy.22736

Tree, D. R., Shulman, J. M., Rousset, R., Scott, M. P., Gubb, D., & Axelrod, J. D. (2002). Prickle mediates feedback amplification to generate asymmetric planar cell polarity signaling. *Cell, 109*(3), 371-381. doi:10.1016/s0092-8674(02)00715-8

Tsurumi, A., Xia, F., Li, J., Larson, K., LaFrance, R., & Li, W. X. (2011). STAT is an essential activator of the zygotic genome in the early Drosophila embryo. *PLoS Genet, 7*(5), e1002086. doi:10.1371/journal.pgen.1002086

Verboogen, D. R. J., Ter Beest, M., Honigmann, A., & van den Bogaart, G. (2018). Secretory vesicles of immune cells contain only a limited number of interleukin 6 molecules. *FEBS Lett, 592*(9), 1535-1544. doi:10.1002/1873-3468.13036

Vinson, C. R., & Adler, P. N. (1987). Directional non-cell autonomy and the transmission of polarity information by the frizzled gene of Drosophila. *Nature, 329*(6139), 549-551. doi:10.1038/329549a0

Vitorino, P., & Meyer, T. (2008). Modular control of endothelial sheet migration. *Genes Dev, 22*(23), 3268-3281. doi:10.1101/gad.1725808

Vonderheit, A., & Helenius, A. (2005). Rab7 associates with early endosomes to mediate sorting and transport of Semliki forest virus to late endosomes. *PLoS Biol, 3*(7), e233. doi:10.1371/journal.pbio.0030233

Wang, Y., Yang, Q., Meng, X., Wijaya, C. S., Ren, X., & Xu, S. (2022). Recruitment of tetraspanin TSP-15 to epidermal wounds promotes plasma membrane repair in C. elegans. *Dev Cell, 57*(13), 1630-1642 e1634. doi:10.1016/j.devcel.2022.06.004

Williams, A. M., Donoughe, S., Munro, E., & Horne-Badovinac, S. (2022). Fat2 polarizes the WAVE complex in trans to align cell protrusions for collective migration. *Elife, 11*. doi:10.7554/eLife.78343

Wong, L. L., & Adler, P. N. (1993). Tissue polarity genes of Drosophila regulate the subcellular location for prehair initiation in pupal wing cells. *J Cell Biol, 123*(1), 209-221. doi:10.1083/jcb.123.1.209

Woodcock, K. J., Kierdorf, K., Pouchelon, C. A., Vivancos, V., Dionne, M. S., & Geissmann, F. (2015). Macrophage-derived upd3 cytokine causes impaired glucose homeostasis and reduced lifespan in Drosophila fed a lipid-rich diet. *Immunity, 42*(1), 133-144.

doi:10.1016/j.immuni.2014.12.023

Wulff, J., & Black, M. J. (2015, 7-12 June 2015). *Efficient sparse-to-dense optical flow estimation using a learned basis and layers.* Paper presented at the 2015 IEEE Conference on Computer Vision and Pattern Recognition (CVPR).

Yang, C. H., Axelrod, J. D., & Simon, M. A. (2002). Regulation of Frizzled by fat-like cadherins during planar polarity signaling in the Drosophila compound eye. *Cell, 108*(5), 675-688. doi:10.1016/s0092-8674(02)00658-x

Yoshihara, M., Adolfsen, B., Galle, K. T., & Littleton, J. T. (2005). Retrograde signaling by Syt 4 induces presynaptic release and synapse-specific growth. *Science, 310*(5749), 858-863. doi:10.1126/science.1117541

Zallen, J. A. (2007). Planar polarity and tissue morphogenesis. *Cell, 129*(6), 1051-1063. doi:10.1016/j.cell.2007.05.050

Zeidler, M. P., Bach, E. A., & Perrimon, N. (2000). The roles of the Drosophila JAK/STAT pathway. *Oncogene, 19*(21), 2598-2606. doi:10.1038/sj.onc.1203482

Zeidler, M. P., Perrimon, N., & Strutt, D. I. (1999). Polarity determination in the Drosophila eye: a novel role for unpaired and JAK/STAT signaling. *Genes Dev, 13*(10), 1342-1353. doi:10.1101/gad.13.10.1342

Zhao, Q., Wirka, R., Nguyen, T., Nagao, M., Cheng, P., Miller, C. L., . . . Quertermous, T. (2019). TCF21 and AP-1 interact through epigenetic modifications to regulate coronary artery disease gene expression. *Genome Med, 11*(1), 23. doi:10.1186/s13073-019-0635-9

Zhao, X., & Karpac, J. (2017). Muscle Directs Diurnal Energy Homeostasis through a Myokine-Dependent Hormone Module in Drosophila. *Curr Biol, 27*(13), 1941-1955 e1946. doi:10.1016/j.cub.2017.06.004

Zheng, H., Yang, X., & Xi, Y. (2016). Fat body remodeling and homeostasis control in Drosophila. *Life Sci, 167*, 22-31. doi:10.1016/j.lfs.2016.10.019

Zhou, B., Feng, C., Sun, S., Chen, X., Zhuansun, D., Wang, D., . . . Feng, J. (2024). Identification of signaling pathways that specify a subset of migrating enteric neural crest cells at the wavefront in mouse embryos. *Dev Cell*. doi:10.1016/j.devcel.2024.03.034

Data availability

The mass spectrometry proteomics data have been deposited to the ProteomeXchange Consortium (https://www.iprox.cn/page/PSV023.html;?url=1708323921277ZyfC) via the iProX partner repository (J. Ma et al., 2019) with accession number gfnR. The RNA-Seq data generated and analyzed in this study have been deposited in the NCBI database under accession number GSE256177 with token code: clyfasuctboflat. The SMART-Seq data (L3, 0hr APF and 2hr APF) analyzed in this study have been deposited in the NCBI database under accession number GSE184856 [https://www.ncbi.nlm.nih.gov/geo/query/acc.cgi?acc=GSE184856]. The ChIP-Seq data generated and analyzed in this study have been deposited in the NCBI database under accession code 256176 with token: qvupguyijvyndyf.

963 **Figure legends**

964 **Figure 1 Fat body affects disciplined migration of tracheal progenitors.** (A)
965 Schematic cartoon showing the migration of tracheal progenitors (red) and
966 degenerative tracheal branches (dashed grey lines) in pupae. Fat body is shown in
967 beige. Arrows denote anterior-posterior (A-P) axis. (B, C) Frontal section (B) and
968 sagittal view (C) showing the relative position of fat body and tracheal progenitors.
969 (D-J') Migration of tracheal progenitors in control and fat body perturbation flies. (D-
970 D'') Migration of tracheal progenitors (red) upward from transverse connective (blue
971 dashed lines) and along the dorsal trunk (white dotted lines) at 0hr APF (D), 1hr APF
972 (D'), and 3hr APF (D''). (E-E'') Bidirectional movement of tracheal progenitors in fat
973 body-depleted (*lsp2>rpr.hid*) flies. 0hr APF (E), 1hr APF (E'), 3hr APF (E''). Arrows
974 point to anterior movement of tracheal progenitors. (F) Bar graph showing the
975 migration distance of tracheal progenitors. Error bars represent SEM. (G-G') The
976 distribution of progenitors at 2hr APF. (H-H'') The distribution of progenitors in fat
977 body-depleted flies at 2hr APF. (I-J') Computer simulation depicting trajectories of
978 progenitor migration. (I, J) Confocal images of tracheal progenitors. (I', J') Vectors of
979 progenitor migration. (K) Bar graph plots the binary entropy that represents the
980 disorderedness of migration direction of tracheal progenitors. (L) The Bernoulli
981 random variable X showing optic flow distribution of the binarized directions in each
982 group. * indicates $p < 0.05$, ** indicates $p < 0.01$, *** indicates $p < 0.001$, and ns
983 indicates not significant. Scale bar: 100 μm (B, C), 200 μm (D-E''). Genotypes: (B,
984 C) *UAS-mCD8-GFP/+; lsp2-Gal4,P[B123]-RFP-moe/+*; (D-D'', G, G')
985 *Gal80^{ts}/+;lsp2-Gal4,P[B123]-RFP-moe/+* ; (E-E'', H, H') *UAS-rpr-*
986 *hid/+;Gal80^{ts}/+;lsp2-Gal4,P[B123]-RFP-moe/+*.
987

988 **Figure 2 Dependence of tracheal progenitors on cytokines from fat body.** (A) Top
989 functional clusters among the differentially expressed genes of progenitors between
990 control and fat body-depleted pupae. (B) Heatmap depicting expression levels of
991 principal target genes of signaling pathways in L3 larvae, 0hr APF pupae and 2hr APF

992 pupae. (C) Heatmap showing the differential expression of target genes of signaling
993 pathways between control and fat body-depleted pupae. (D-D'') Migration of tracheal
994 progenitors along the dorsal trunk at 0hr APF (D), 1hr APF (D'), and 3hr APF (D'').
995 The white dashed line shows transverse connective. (E-E''). Migration of tracheal
996 progenitors in *upd2RNAi* flies. (F) Bar graph plots the migration distance of tracheal
997 progenitors. Error bars represent SEM. (G) Volcano plot showing surface proteomics
998 of tracheal epithelium (up-regulated genes with ten-fold or higher changes in red;
999 down-regulated genes with ten-fold or higher changes in blue). (H) Top functional
1000 classes among the surface proteomics of trachea. (I) Schematic diagram depicting the
1001 working principle of the DIPF reporter. (J) The expression of DIPF reporter in
1002 tracheal progenitors. The progenitors are outlined by dashed lines. * indicates $p <$
1003 0.05, ** indicates $p < 0.01$, *** indicates $p < 0.001$, and ns indicates not significant.
1004 Scale bar: 200 μm (D-E''), 50 μm (J). Genotypes: (D-D'') *lsp2-Gal4,P[B123]-RFP-*
1005 *moe/+*; (E-E'') *lsp2-Gal4,P[B123]-RFP-moe/UAS-upd2RNAi*; (J) *btl-Gal4/UAS-*
1006 *DIPF*.
1007
1008 **Figure 3 JAK/STAT pathway is required for the discipline of tracheal progenitor**
1009 **migration.** (A-D'') Migration of tracheal progenitors along the dorsal trunk at 0hr
1010 APF, 1hr APF and 3hr APF. The white dashed line shows transverse connective. The
1011 progenitors of control (A-A''), *domeRNAi* (B-B''), *hopRNAi* (C-C''), and
1012 *stat92ERNAi* (D-D'') flies. (E) Bar graph showing migration distance of progenitors.
1013 Error bars represent SEM. (F-G'') JAK inhibition causes bidirectional movement of
1014 progenitors. Migration of tracheal progenitors in the absence (DMSO-fed) (F-F'') or
1015 in the presence of Tofacinib (JAK inhibitor) (G-G''). (H) Bar graph showing the
1016 distance of anterior movement. Error bars represent SEM. (I-L) The expression of
1017 Stat92E-GFP in tracheal progenitors of control (I), *domeRNAi* (J), *hopRNAi* (K) and
1018 *stat92ERNAi* (L) flies. The progenitors are outlined by dashed lines. (M, N) The
1019 expression of Stat92E-GFP in tracheal progenitors of control (M) or *upd2RNAi* flies
1020 (N). (O, P) The expression of Stat92E-GFP in tracheal progenitors of DMSO-fed
1021 (control, O) or Tofacinib-treated (P) flies. Dashed lines outline tracheal progenitors.

1022 (Q) Bar graph plots relative signals of Stat92E-GFP reporter. Error bars represent
1023 SEM. * indicates $p < 0.05$, ** indicates $p < 0.01$, *** indicates $p < 0.001$, and ns
1024 indicates not significant. Scale bar: 200 μm (A-D'', F-G''), 50 μm (I-P). Genotypes:
1025 (A-A'', F-G'') *btl-Gal4/+;P[B123]-RFP-moe/+*; (B-B'') *btl-Gal4/+;P[B123]-RFP-*
1026 *moe/UAS-domeRNAi*; (C-C'') *btl-Gal4/+;P[B123]-RFP-moe/UAS-hopRNAi*; (D-D'')
1027 *btl-Gal4/+;P[B123]-RFP-moe/UAS-stat92ERNAi*; (I) *btl-Gal4,Stat92E-GFP/+*; (J)
1028 *btl-Gal4,Stat92E-GFP/+;UAS-domeRNAi/+*; (K) *btl-Gal4,Stat92E-GFP/+;UAS-*
1029 *hopRNAi/+*; (L) *btl-Gal4,Stat92E-GFP/+;UAS-Stat92ERNAi/+*; (M, O, P) *Stat92E-*
1030 *GFP/+; lsp2-Gal4/+*; (N) *Stat92E-GFP/+;lsp2-Gal4/UAS-upd2RNAi*.
1031
1032 **Figure 4 Identification of gene targets of Stat92E in *Drosophila* tracheal**
1033 **progenitors.** (A) Bubble plot represents the top functional clusters among gene
1034 targets. The establishment of planar polarity denoted in red solid box is identified with
1035 high enrichment score. (B) Top functional classes among the differentially expressed
1036 genes in larval-pupal transition. (C) ChIP-seq peaks at loci regulated by Stat92E.
1037 Scale bar: 20kb (*ds*, *fz*, *stan*), 5kb (*fat2*, *vg*), 1kb (*fj*). (D-H) Validation of gene targets
1038 of Stat92E ChIP-seq. (D-G) The expression of Ds-GFP in the tracheal progenitors of
1039 control (D), *domeRNAi* (E), *hopRNAi* (F) and *stat92ERNAi* (G). The progenitors are
1040 outlined by dashed lines. (H) The bar graphs plot the relative level of Ds. Error bars
1041 represent SEM. (I-M) The expression of Fj in tracheal progenitors. The expression of
1042 Fj-GFP in the tracheal progenitors of control (I), *domeRNAi* (J), *hopRNAi* (K) and
1043 *stat92ERNAi* (L). Dashed lines outline tracheal progenitors. (M) The bar graphs plot
1044 the relative level of Fj. Error bars represent SEM. (N-R) The level of Ft-GFP in the
1045 tracheal progenitors of control (N), *domeRNAi* (O), *hopRNAi* (P) and *stat92ERNAi*
1046 (Q). (R) The bar graphs plot the relative level of Ft. Error bars represent SEM. Scale
1047 bar: 50 μm (D-G, I-L, N-Q). Genotypes: (D) *btl-Gal4,Ds-GFP/+*; (E) *btl-Gal4,Ds-*
1048 *GFP/+;UAS-domeRNAi/+*; (F) *btl-Gal4,Ds-GFP/+;UAS-hopRNAi/+*; (G) *btl-*
1049 *Gal4,Ds-GFP/+;UAS-stat92ERNAi/+*; (I) *btl-Gal4,Fj-GFP/+*; (J) *btl-Gal4,Fj-*
1050 *GFP/+;UAS-domeRNAi/+*; (K) *btl-Gal4,Fj-GFP/+;UAS-hopRNAi/+*; (L) *btl-*
1051 *Gal4,Fj-GFP/+;UAS-stat92ERNAi/+*; (N) *btl-Gal4/+;Ft-GFP/+*; (O) *btl-Gal4/+;Ft-*

1052 *GFP/UAS-domeRNAi*; (P) *btl-Gal4/+;Ft-GFP/UAS-hopRNAi*; (Q) *btl-Gal4/+;Ft-*
1053 *GFP/UAS-stat92ERNAi*.
1054
1055 **Figure 5 Disciplined migration requires planar cell polarity system.** (A-E)
1056 Migration of tracheal progenitors. The migration of progenitors in control (A-A''),
1057 *dsRNAi* (B-B''), *ftRNAi* (C-C'') and *fjRNAi* (D-D'') flies. (E) Bar graph plots the
1058 migration distance of anterior movement. (F-I) Level of Ft in tracheal progenitors of
1059 control (F, G) and *stat92ERNAi* (H-J) flies. The images show progenitors at 1hr APF
1060 (H, H') and 2hr APF (I, I'). Ft-GFP (green) (F, H, I), phalloidin (magenta), Hoechst
1061 (blue), and merged images (F', H', I'). (G, J) Profile plots showing the level of Ft-
1062 GFP in control (G) and *stat92ERNAi* (J) flies. The levels of Ft were measured along
1063 the dotted lines in F' or I'. Anterior (A) and posterior (P). (K) Representative traces
1064 plot the migration distance relative to the origin. (K') Rose plot depicting the direction
1065 of cell movement. (L) Representative traces showing the movement of individual *fj*-
1066 KO cells relative to their origin. (L') Rose plot depicting the movement direction of *fj*-
1067 KO cells. (M) Scatter plots represent the ratio (*d*/*D*) of straight-line length
1068 displacement (*d*) relative to the length of the migration track (*D*) of individual cell.
1069 Error bars represent SEM. * indicates $p < 0.05$, ** indicates $p < 0.01$, *** indicates p
1070 < 0.001, and ns indicates not significant. Scale bar: 200 μm (A-D''), 50 μm (F, F'),
1071 100 μm (H-I'). Genotypes: (A-A'') *btl-Gal4/+;P[B123]-RFP-moe/+*; (B-B'') *btl-*
1072 *Gal4/UAS-dsRNAi;P[B123]-RFP-moe/+*; (C-C'') *btl-Gal4/+;P[B123]-RFP-*
1073 *moe/UAS-ftRNAi*; (D-D'') *btl-Gal4/UAS-fjRNAi;P[B123]-RFP-moe/+*; (F, F') *btl-*
1074 *Gal4/+;Ft-GFP/+*; (H, H', I, I') *btl-Gal4/+;Ft-GFP/UAS-stat92ERNAi*.
1075
1076 **Figure 6 The production and transport of Upd2 from fat body.** (A, B) Upd2-
1077 mCherry-containing vesicles in fat body of control (DMSO-fed, A) and BFA-treated
1078 L3 larvae (B). (C) Bar graph plots the abundance of Upd2-mCherry-containing
1079 vesicles in fat body. Error bars represent SEM. (D, E) The confocal image showing
1080 the Upd2-containing vesicles in progenitors of DMSO-fed control (D) and BFA-
1081 treated flies (E). (F) Bar graph plots the abundance of Upd2-mCherry-containing

1082 vesicles in progenitors. (G) Upd2-mCherry containing vesicles (red) in fat body. (H, I)
1083 Upd2 accumulation in fat body was increased in the presence of *grasp65RNAi* (H)
1084 and *lbmRNAi* (I). (J) Bar graph plots the abundance of Upd2-mCherry-containing
1085 vesicles. Error bars represent SEM. (K-M) The Upd2 vesicles (red) in tracheal
1086 progenitors (DAPI) in control (K), *grasp65RNAi* (L) and *lbmRNAi* (M) flies. Dashed
1087 lines outline tracheal progenitors. (N) Bar graph plots the abundance of Upd2-
1088 mCherry-containing vesicles in progenitors. Error bars represent SEM. * indicates $p <$
1089 0.05, ** indicates $p < 0.01$, *** indicates $p < 0.001$, and ns indicates not significant.
1090 Scale bar: 20 μm (A, B, G-I), 50 μm (D, E, K-M). Genotypes: (A-G, K) *UAS-upd2-*
1091 *mCherry/+;lsp2-Gal4/+*; (H, L) *UAS-upd2-mCherry/UAS-grasp65RNAi;lsp2-Gal4/+*;
1092 (I, M) *UAS-upd2-mCherry/+;lsp2-Gal4/UAS-lbmRNAi*.
1093
1094 **Figure 7 The dependence of tracheal progenitors on vesicle trafficking.** (A-E)
1095 The expression of Stat92E-GFP in tracheal progenitors of control (A), *grasp65RNAi*
1096 (B), *lbmRNAi* (C), *rab5RNAi* (D) and *rab7RNAi* (E) flies. The progenitors are
1097 outlined by dashed lines. (F) Bar graph plots the relative expression of Stat92E-GFP.
1098 Error bars represent SEM. (G, H) The expression of Stat92E-GFP in tracheal
1099 progenitors in DMSO-fed (G) and BFA-treated (H) flies. (I) Bar graph plots the
1100 relative expression of Stat92E-GFP. Error bars represent SEM. (J) The signal of DIPF
1101 reporter in tracheal progenitors. (K) The effects of Tofacinib (JAK inhibitor) on DIPF
1102 reporter in progenitors. (L) The effects of Brefeldin A on DIPF reporter in progenitors.
1103 Dashed lines outline tracheal progenitors. (M) Bar graphs showing the signal of DIPF
1104 reporter. Error bars represent SEM. (N-O'') Migration of tracheal progenitors in
1105 DMSO-fed flies (N-N'') and BFA-treated flies (O-O''). (P) Bar graph plots migration
1106 distance of anterior movement. Error bars represent SEM. (Q-U'') Migration of
1107 tracheal progenitors at 0hr APF (Q), 1hr APF (Q'), 3hr APF (Q''). The confocal
1108 images showing the tracheal progenitors in control (Q-Q''), *grasp65RNAi* (R-R''),
1109 *lbmRNAi* (S-S''), *rab5RNAi* (T-T'') and *rab7RNAi* (U-U'') flies. (V) Bar graph plots
1110 the migration distance of anterior movement. Error bars represent SEM. * indicates p
1111 < 0.05, ** indicates $p < 0.01$, *** indicates $p < 0.001$, and ns indicates not significant.

1112 Scale bar: 50 μm (A-E, G, H, J-L), 200 μm (N-O'', Q-U''). Genotypes: (A, G, H)
1113 *lsp2-Gal4,Stat92E-GFP/+*; (B) *UAS-grasp65RNAi/+;lsp2-Gal4,Stat92E-GFP/+*; (C)
1114 *lsp2-Gal4,Stat92E-GFP/UAS-lbmRNAi*; (D) *UAS-rab5RNAi/+;lsp2-Gal4,Stat92E-*
1115 *GFP/+*; (E) *UAS-rab7RNAi/+;lsp2-Gal4,Stat92E-GFP/+*; (J-L) *btl-Gal4/UAS-DIPF*;
1116 (N-Q'') *lsp2-Gal4,P[B123]-RFP-moe/+*; (R-R'') *lsp2-Gal4,P[B123]-RFP-moe/UAS-*
1117 *grasp65RNAi*; (S-S'') *lsp2-Gal4,P[B123]-RFP-moe/+;UAS-lbmRNAi/+*; (T-T'')
1118 *UAS-rab5RNAi/+;lsp2-Gal4,P[B123]-RFP-moe/+*; (U-U'') *UAS-rab7RNAi/+;lsp2-*
1119 *Gal4,P[B123]-RFP-moe/+*.
1120
1121 **Figure 8 The roles of endocytic trafficking system in the transport of Upd2.** (A-
1122 D''') The confocal images showing the colocalization between Upd2 (red) (A, B, C,
1123 D) and Rab5 (GFP) (A'), Rab7 (GFP) (B'), Grasp65 (GFP) (C') or Lbm (GFP). (A'',
1124 B'', C'', D'') Merged images. (D''') 3D high-magnification view of the boxed inset in
1125 D''. (D'''') The Pearson's correlation coefficient depicting colocalization between
1126 Lbm and Upd2 in fat body cells. (E-J) The PLA (Proximity Ligation Assay) assay
1127 showing the interaction between Upd2 and Rab5 (E, F), Rab7 (G, H) or Lbm (I, J).
1128 (K-M) Co-immunoprecipitation assay showing physical interaction between Upd2
1129 and Rab5 (K), Rab7 (L) or Lbm (M) in larval fat body. (N-T) The expression of Lbm-
1130 pHluorin in larval fat body and progenitors of control (N, O), *rab5RNAi* (P, Q) and
1131 *rab7RNAi* (R, S) flies. Dashed lines outline tracheal progenitors. Arrowheads point to
1132 Lbm-pHluorin puncta. (T) Schematic diagram depicting Upd2-operated disciplined
1133 migration of tracheal progenitors. Scale bar: 5 μm (A-D'', E-J), 10 μm (N, P, R), 20
1134 μm (O, Q, S). Genotypes: (A-A'', E, F) *UAS-upd2-mCherry/+;lsp2-Gal4/UAS-GFP-*
1135 *rab5*; (B-B'', G, H) *UAS-upd2-mCherry/+;lsp2-Gal4/UAS-GFP-rab7*; (C-C'') *UAS-*
1136 *upd2-mCherry/UAS-grasp65-GFP;lsp2-Gal4/+*; (D-D'''', I-L) *UAS-upd2-*
1137 *mCherry/UAS-lbm-GFP;lsp2-Gal4/+*; (N, O) *UAS-lbm-pHluorin/+;lsp2-Gal4/+*; (P,
1138 Q) *UAS-lbm-pHluorin/UAS-rab5RNAi;lsp2-Gal4/+*; (R, S) *UAS-lbm-pHluorin/UAS-*
1139 *rab7RNAi;lsp2-Gal4/+*.
1140
1141 **Figure 1-figure supplement 1 Genetic perturbation of fat body by expression of**

1142 **pro-apoptotic genes, *rpr* and *hid*.** Confocal images of larval fat body in control (A)
1143 and *lsp2>rpr.hid* (B) animals. Microscopic pictures of control (C) and *lsp2>rpr.hid*
1144 larvae (D). (E) Scatter plot showing migration velocity of tracheal progenitors in
1145 control and *lsp2>rpr.hid* animals. (F, G) The incorporation of EdU in the tracheal
1146 progenitors of control (F) and *lsp2>rpr.hid* animals (G). (H) Bar graph depicting the
1147 number of EdU incorporation. Scale bar: 100 μm (A, B), 20 μm (C, D), 50 μm (F, G).
1148 Genotypes: (A, C, F) *lsp2-Gal4,P[B123]-RFP-moe/+*; (B, D) *UAS-rpr.hid/+;lsp2-*
1149 *Gal4,P[B123]-RFP-moe/+*; (G) *UAS-rpr.hid/+;Gal80^{ts}/+;lsp2-Gal4,P[B123]-RFP-*
1150 *moe/+*.
1151
1152 **Figure 2-figure supplement 1 Identification of genes that contribute to**
1153 **progenitors migration.** (A) Differentially expressed genes in tracheal progenitors of
1154 *lsp2>rpr.hid* pupa compared with control. (B) Volcano plot of RNA-seq showing
1155 differentially regulated genes with 2-fold or higher changes (up-regulated genes in
1156 red; down-regulated genes in blue) in *lsp2>rpr.hid* compared with control. (C-I'') The
1157 migration of progenitors at 0hr APF, 1hr APF, or 3hr APF in control (C-C'') and
1158 *upd1RNAi* (D-D''), *upd3RNAi* (E-E''), *pvf1RNAi* (F-F''), *pvf2RNAi* (G-G''), *pvf3RNAi*
1159 (H-H''), and *hhRNAi* (I-I''). (J) Bar graph represents the migration distance of anterior
1160 movement. Error bars represent SEM. (K) The migration of progenitors in control (K-
1161 K'') and *btl>upd2RNAi* (L-L''). (M) Bar graph plots the migration distance of anterior
1162 movement. Error bars represent SEM. * indicates $p < 0.05$, ** indicates $p < 0.01$, ***
1163 indicates $p < 0.001$, and ns indicates not significant. Scale bar: 200 μm (C-I'', K-L'').
1164 Genotypes: (C-C'') *lsp2-Gal4,P[B123]-RFP-moe/+*; (D-D'') *lsp2-Gal4,P[B123]-*
1165 *RFP-moe/UAS-upd1RNAi*; (E-E'') *lsp2-Gal4,P[B123]-RFP-moe/UAS-upd3RNAi*; (F-
1166 F'') *lsp2-Gal4,P[B123]-RFP-moe/UAS-pvf1RNAi*; (G-G'') *lsp2-Gal4,P[B123]-RFP-*
1167 *moe/UAS-pvf2RNAi*; (H-H'') *lsp2-Gal4,P[B123]-RFP-moe/UAS-pvf3RNAi*; (I-I'')
1168 *lsp2-Gal4,P[B123]-RFP-moe/UAS-hhRNAi*; (K-K'') *btl-Gal4/+;P[B123]-RFP-*
1169 *moe/+*; (L-L'') *btl-Gal4/+;P[B123]-RFP-moe/UAS-upd2RNAi*.
1170
1171 **Figure 2-figure supplement 2 Surface proteomics of *Drosophila* trachea.** (A-C)

1172 Representative confocal images showing the trachea of *btl>CD2-HRP* flies after
1173 oxidation reaction in the presence of both BXXP and H_2O_2 (A), BXXP only (B), or
1174 H_2O_2 only (C). (D) The western blot showing the biotinylated proteins labeled by an
1175 HRP-catalyzed reaction with both BXXP and H_2O_2. (E) The confocal image showing
1176 the trachea of *dome>GFP* flies. The expression domain of *dome* is visualized by
1177 *dome*-Gal4-controlled GFP expression. The progenitors labeled by a progenitor-
1178 specific enhancer, P[B123]-RFP-moe are outlined by dashed lines. The overlapping
1179 expression of GFP and P[B123]-RFP-moe. (F-H) The expression of Upd2 cytokines
1180 in various tissues. (F, G) The expression of *upd>GFP* in trachea (F) and fat body (G).
1181 It was obvious in fat body, but barely detectable in trachea. The tracheal progenitors
1182 were outlined by dashed lines. (H) Heatmap showing the relative level of *upd2*
1183 expression in different tissue. mRNA levels of upd2 were quantitatively measured by
1184 qRT-PCR. Scale bar: 50 μm (E, F), 100 μm (G). Genotypes: (A-C) *btl-Gal4/UAS-*
1185 *CD2-HRP*; (E) *dome-Gal4/+;UAS-GFP/P[B123]-RFP-moe*; (F, G) *upd-Gal4/UAS-*
1186 *GFP*.
1187
1188 **Figure 4-figure supplement 1 Annotation and analysis of genomic occupancy of**
1189 **Stat92E.** (A-C) Pie chart (A, B) and histogram (C) depicting the distribution of ChIP-
1190 seq peaks relative to the nearby annotated genes. (D) Peaks of Stat92E association in
1191 the promotor regions of *yurt* and *crb*. Scale bar: 2kb for *yurt*, 5kb for *crb*. (E) Relative
1192 enrichment of JAK/STAT target genes analyzed by ChIP-qPCR. (F-I) The expression
1193 of Fat2-GFP in the tracheal progenitors of control (F), *domeRNAi* (G), *hopRNAi* (H)
1194 and *stat92ERNAi* (I). The progenitors are outlined by dashed lines. (J) The bar graphs
1195 plot the relative level of Fat2. Error bars represent SEM. (K-N) The expression of Yurt
1196 in tracheal progenitors. The expression of Yurt-GFP in the tracheal progenitors of
1197 control (K), *domeRNAi* (L), *hopRNAi* (M) and *stat92ERNAi* (N). The progenitors are
1198 outlined by dashed lines. (O) The bar graphs plot the relative level of Yurt. Error bars
1199 represent SEM. (P-S) The expression of Crb-GFP in the tracheal progenitors of
1200 control (P), *domeRNAi* (Q), *hopRNAi* (R) and *stat92ERNAi* (S). The progenitors are
1201 outlined by dashed lines. (T) The bar graphs plot the relative level of Crb. Error bars

1202 represent SEM. (U) The expression of JAK/STAT targets in the trachea of
1203 *stat92ERNAi* flies. Quantitative RT-PCR was performed in triplets to analyze the
1204 mRNA level. The expression levels in *stat92ERNAi* larvae were presented relative to
1205 *Gal4* control. * indicates $p < 0.05$, ** indicates $p < 0.01$, *** indicates $p < 0.001$, and
1206 ns indicates not significant. Scale bar: 50 μm (F-I, K-N, P-S). Genotypes: (F) *btl-*
1207 *Gal4,Fat2-GFP/+*; (G) *btl-Gal4,Fat2-GFP/+;UAS-domeRNAi/+*; (H) *btl-Gal4,Fat2-*
1208 *GFP/+;UAS-hopRNAi/+*; (I) *btl-Gal4,Fat2-GFP/+;UAS-stat92ERNAi/+*; (J) *btl-*
1209 *Gal4/+;Yurt-GFP/+*; (K) *btl-Gal4/+;Yurt-GFP/UAS-domeRNAi*; (L) *btl-Gal4/+;Yurt-*
1210 *GFP/UAS-hopRNAi*; (M) *btl-Gal4/+;Yurt-GFP/UAS-stat92ERNAi*; (P) *btl-*
1211 *Gal4/+;Crb-GFP/+*; (Q) *btl-Gal4/+;Crb-GFP/UAS-domeRNAi*; (R) *btl-Gal4/+;Crb-*
1212 *GFP/UAS-hopRNAi*; (S) *btl-Gal4/+;Crb-GFP/UAS-stat92ERNAi*.
1213
1214 **Figure 4-figure supplement 2 Ds alters the level of Ft.** (A-C) The level of Ft-GFP
1215 in control (A), UAS-ds (B), and dsRNAi (C) flies. (D) Bar graph represents the signal
1216 of Ft-GFP. Error bars represent SEM. ****indicates $p < 0.0001$. Scale bar: 50 μm (A-
1217 C). Genotypes: (A) *btl-Gal4/+;Ft-GFP/+*; (B) *btl-Gal4/+;Ft-GFP/UAS-ds*; (C) *btl-*
1218 *Gal4/+;Ft-GFP/UAS-dsRNAi*.
1219
1220 **Figure 5-figure supplement 1 Apico-basal polarity proteins contribute to the**
1221 **migration polarity of progenitors.** (A-H'') The migration of progenitors at 0hr APF
1222 (A), 1hr APF (A'), 3hr APF (A'') in control (A-A''), *UAS-ds* (B-B''), *UAS-ft* (C-C''),
1223 *fat2RNAi* (E-E''), *crbRNAi* (F-F''), *yurtRNAi* (G-G'') and *scbRNAi* (H-H''). (D, I) Bar
1224 graph plots the migration distance of anterior movement. Error bars represent SEM. *
1225 indicates $p < 0.05$, ** indicates $p < 0.01$, *** indicates $p < 0.001$, and ns indicates not
1226 significant. Scale bar: 200 μm (A-C'', E-H''). Genotypes: (A-A'') *btl-*
1227 *Gal4/+;P[B123]-RFP-moe/+*; (B-B'') *btl-Gal4/+;P[B123]/UAS-ds*; (C-C'') *btl-*
1228 *Gal4/UAS-ft;P[B123]/+*; (E-E'') *btl-Gal4/+;P[B123]-RFP-moe/UAS-fat2RNAi*; (F-
1229 F'') *btl-Gal4/+;P[B123]-RFP-moe/UAS-crbRNAi*; (G-G'') *btl-Gal4/+;P[B123]-RFP-*
1230 *moe/UAS-yurtRNAi*; (H-H'') *btl-Gal4/+;P[B123]-RFP-moe/UAS-scbRNAi*.
1231

1232 **Figure 5-figure supplement 2 Protrusions extending from the leading edge of**
1233 **progenitors.** (A, B) The confocal image showing the filopodia at the leading edge of
1234 migrating tracheal progenitors in control (A) and *upd2RNAi* flies (B). Arrows denote
1235 anterior-posterior (A-P) axis. Dashed lines indicate dorsal trunk. (C) Bar graph
1236 depicting the number of filopodia extending from leading edge. (D, E) Expression of
1237 *bnl*-lacZ in the trachea of control (D) and *stat92ERNAi* (E) flies. Scale bar: 100 μm
1238 (A, B), 500 μm (D, E). Genotypes: (A) *lsp2-Gal4,P[B123]-RFP-moe/+*; (B) *lsp2-*
1239 *Gal4,P[B123]-RFP-moe/UAS-upd2RNAi*.
1240
1241 **Figure 5-figure supplement 3 The dependence of migration directionality on**
1242 **Ft/Ds system.** (A) Representative traces plot the migration distance relative to the
1243 origin. (B) Rose plot depicting the direction of cell movement. (C) Representative
1244 traces showing the movement of individual *dsRNAi* cells relative to their origin. (D)
1245 Rose plot depicting the movement direction of *dsRNAi* cells. (E) Representative traces
1246 showing the movement of individual *ftRNAi* cells relative to their origin. (F) Rose plot
1247 depicting the movement direction of *ftRNAi* cells. (G) Scatter plots represent the ratio
1248 (d/D) of straight-line length displacement (d) relative to the length of the migration
1249 track (D) of individual cell.
1250
1251 **Figure 7-figure supplement 1 The roles of Rabs in transport of Upd2**. (A-F'')
1252 Migration of tracheal progenitors. The migration of progenitors at 0hr APF, 1hr APF,
1253 3hr APF in control (A-A''), *rab2RNAi* (B-B''), *rab3RNAi* (C-C''), *rab5RNAi* (D-D'')
1254 and *rab7RNAi* (E-E''). (F) Bar graph plots the migration distance of anterior
1255 movement. Error bars represent SEM. (G-G'') The confocal images showing the
1256 colocalization between Upd2 (red) (G) and Rab3 (GFP) (G'). (G'') Merged images. *
1257 indicates $p < 0.05$, ** indicates $p < 0.01$, *** indicates $p < 0.001$, and ns indicates not
1258 significant. Scale bar: 200 μm (A-E''), 5 μm (G-G''). Genotypes: (A-A'') *lsp2-*
1259 *Gal4,P[B123]-RFP-moe/+*; (B-B'') *lsp2-Gal4,P[B123]-RFP-moe/UAS-rab2RNAi*;
1260 (C-C'') *lsp2-Gal4,P[B123]-RFP-moe/UAS-rab3RNAi*; (D-D'') *lsp2-Gal4,P[B123]-*
1261 *RFP-moe/UAS-rab5RNAi*; (E-E'') *lsp2-Gal4,P[B123]-RFP-moe/UAS-rab7RNAi*; (G-

1262 G'') *UAS-upd2-mCherry/UAS-rab3-YFP;lsp2-Gal4/+*.

1263

1264 **Figure 8-figure supplement 1 Vesicular transport of Upd2.** (A-C'') Co-
1265 localization and interaction between Lbm and Upd2. Co-transfection of act-Gal4,
1266 UAS-lbm-GFP (A) and UAS-upd2-mCherry (A') in S2 cells. (A'') Merged image. (B-
1267 C'') Confocal images showing that Lbm co-localizes with Upd2 in vesicles along the
1268 protrusions of S2 cell. (D) Co-immunoprecipitation assay showing the interaction
1269 between Lbm and Upd2 in S2 cells. (E) Expression of Lbm-pHluorin in larval fat
1270 body, surface view of Lbm-pHluorin. (F) The confocal image showing the expression
1271 Lbm-pHluorin in tracheal progenitors. (G-H) The expression of Lbm-pHluorin in fat
1272 body (G-G') and trachea (H) of BFA-treated flies. The tracheal progenitors were
1273 outlined by dashed lines. Scale bar: 10 μm (A-A'', E, G, G'), 20 μm (F, H).
1274 Genotypes: (E-H) *UAS-lbm-pHluorin/+;lsp2-Gal4/+*.

1275

1276 **Video 1 3D-view of confocal image stacks of tracheal progenitors and fat body.**
1277 Scale bar: 100 μm. Genotypes: *UAS-mCD8-GFP/+;lsp2-Gal4,P[B123]-RFP-moe/+*.

1278

1279 **Video 2 The movement of tracheal progenitors in control and *rpr.hid* flies.** Scale
1280 bar: 100 μm. Genotypes: *Gal80^{ts}/+;lsp2-Gal4,P[B123]-RFP-moe/+* (control) and
1281 *UAS-rpr-hid/+;Gal80^{ts}/+;lsp2-Gal4,P[B123]-RFP-moe/+*.

1282

1283 **Video 3 The movement of tracheal progenitors in control and *upd2RNAi* flies.**
1284 Scale bar: 100 μm. Genotypes: *lsp2-Gal4,P[B123]-RFP-moe/+* (control) and *lsp2-*
1285 *Gal4,P[B123]-RFP-moe/UAS-upd2RNAi*.

1286

1287 **Video 4 The movement of tracheal progenitors in control and JAK/STAT**
1288 **pathway-perturbed flies.** Scale bar: 100 μm. Genotypes: *btl-Gal4/+;P[B123]-RFP-*
1289 *moe/+* (control), *btl-Gal4/+;P[B123]-RFP-moe/UAS-domeRNAi*, *btl-*
1290 *Gal4/+;P[B123]-RFP-moe/UAS-hopRNAi* and *btl-Gal4/+;P[B123]-RFP-moe/UAS-*
1291 *stat92ERNAi*.

1292

1293 **Video 5 The movement of tracheal progenitors in control and PCP component**

1294 **aberrant flies.** Scale bar: 100 μm. Genotypes: *btl-Gal4/+;P[B123]-RFP-*

1295 *moe/+*(control), *btl-Gal4/UAS-dsRNAi;P[B123]-RFP-moe/+* and *btl-*

1296 *Gal4/+;P[B123]-RFP-moe/UAS-ftRNAi*.

1297

1298 **Video 6 The movement of tracheal progenitors in control and *lbmRNAi* flies.**

1299 Scale bar: 100 μm. Genotypes: *lsp2-Gal4,P[B123]-RFP-moe/+* (control) and *lsp2-*

1300 *Gal4,P[B123]-RFP-moe/+;UAS-lbmRNAi/+*.

1301

1302

Figure 1

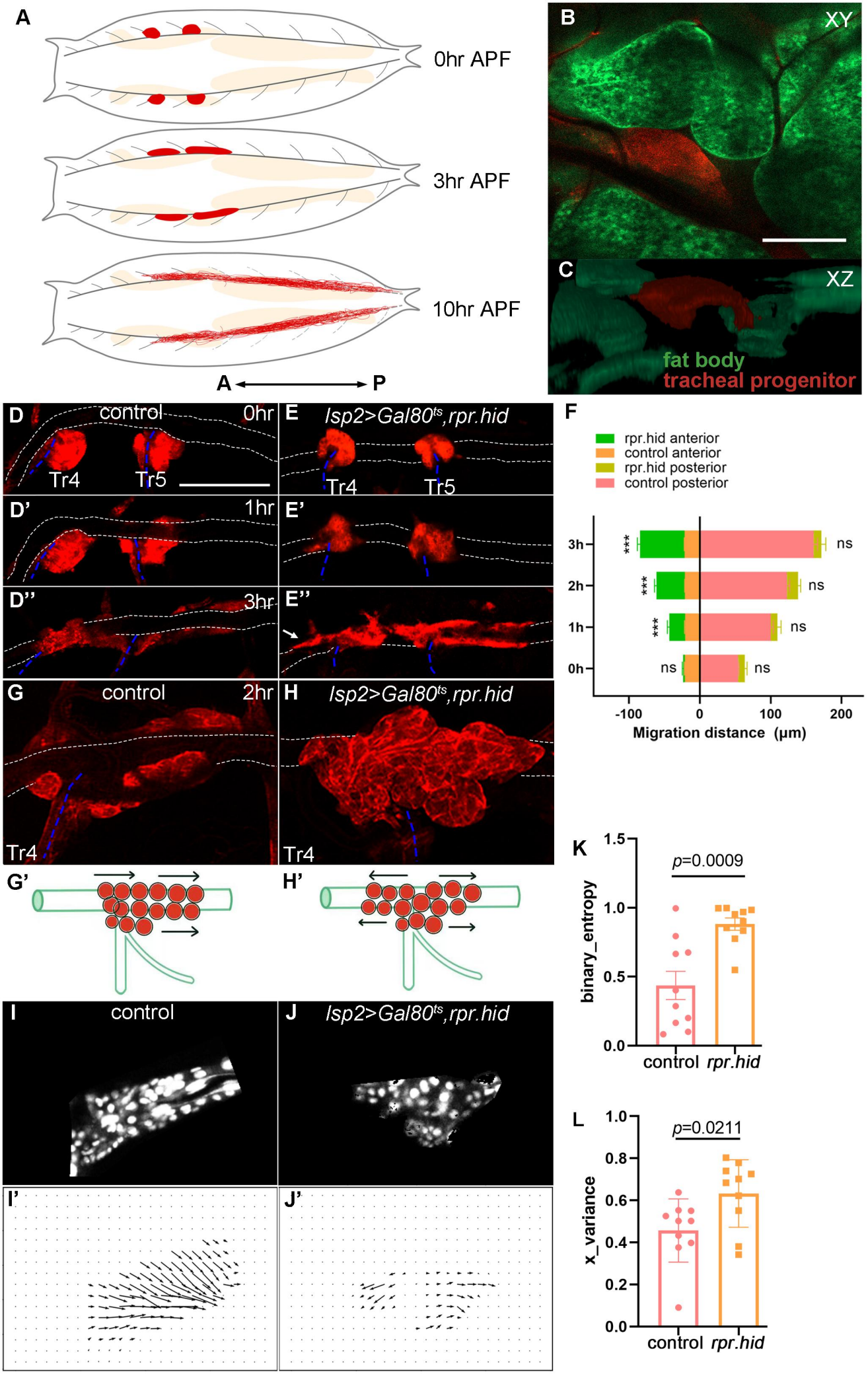
A
0hr APF
3hr APF
10hr APF
A
P
B
XY
C
XZ
fat body
tracheal progenitor
D
control
0hr
Tr4
Tr5
E
lsp2>Gal80ts,rpr.hid
Tr4
Tr5
D'
1hr
E'
D''
3hr
E''
G
control
2hr
Tr4
H
lsp2>Gal80ts,rpr.hid
Tr4
G'
H'
I
control
J
lsp2>Gal80ts,rpr.hid
I'
J'
F
rpr.hid anterior
control anterior
rpr.hid posterior
control posterior
3h
2h
1h
0h
***
ns
-100
0
100
200
Migration distance (μm)
K
p=0.0009
binary_entropy
1.5
1.0
0.5
0.0
control
rpr.hid
L
p=0.0211
x_variance
1.0
0.8
0.6
0.4
0.2
0.0
control
rpr.hid

Figure 2

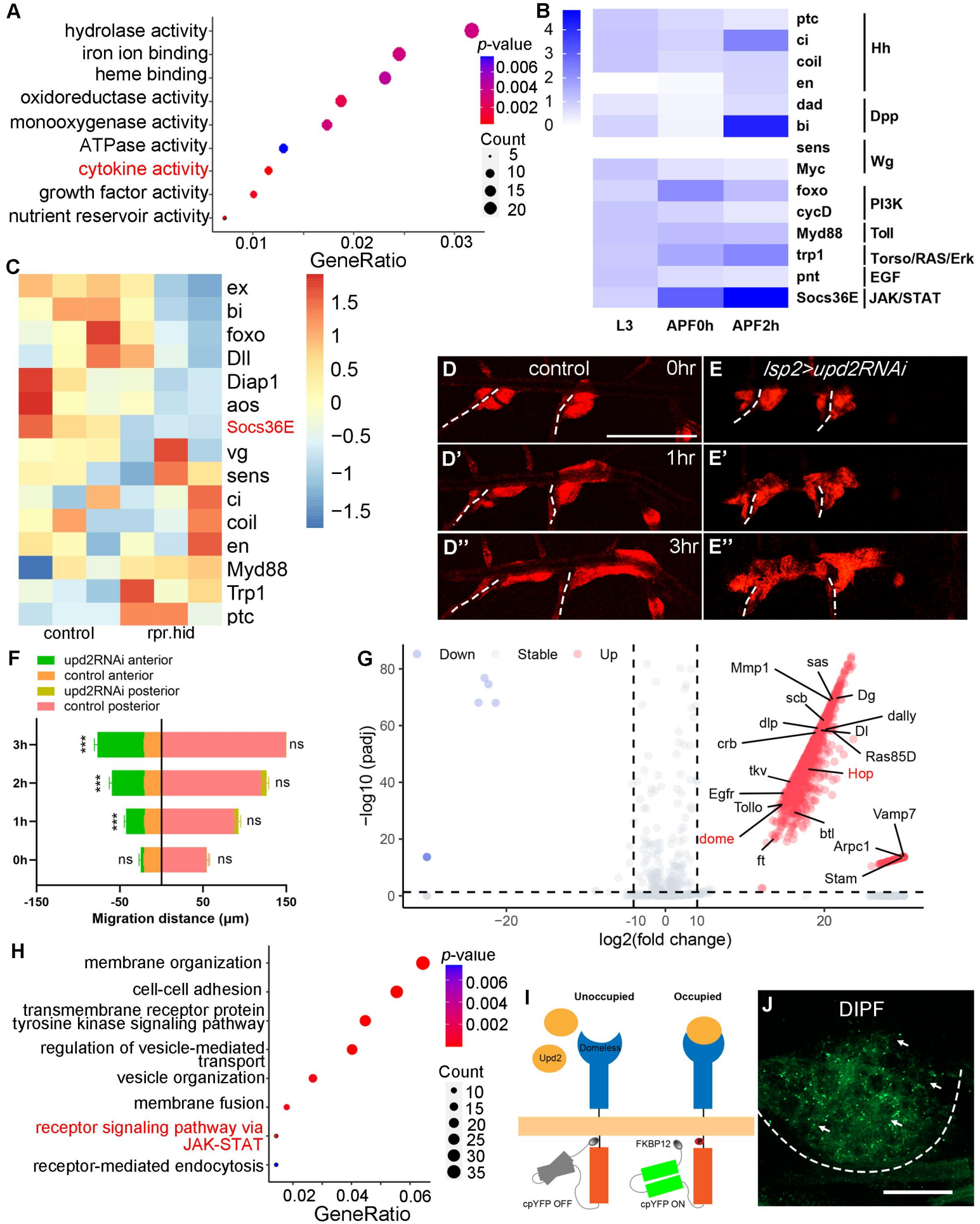
A
hydrolase activity
iron ion binding
heme binding
oxidoreductase activity
monooxygenase activity
ATPase activity
cytokine activity
growth factor activity
nutrient reservoir activity
0.01
0.02
0.03
GeneRatio
p-value
0.006
0.004
0.002
Count
5
10
15
20
B
ptc
ci
coil
en
dad
bi
sens
Myc
foxo
cycD
Myd88
trp1
pnt
Socs36E
Hh
Dpp
Wg
PI3K
Toll
Torso/RAS/Erk
EGF
JAK/STAT
L3
APF0h
APF2h
C
ex
bi
foxo
Dll
Diap1
aos
Socs36E
vg
sens
ci
coil
en
Myd88
Trp1
ptc
control
rpr.hid
1.5
1
0.5
0
−0.5
−1
−1.5
D
control
0hr
D'
1hr
D''
3hr
E
/sp2>upd2RNAi
E'
E''
F
upd2RNAi anterior
control anterior
upd2RNAi posterior
control posterior
3h
2h
1h
0h
***
ns
-150
-50
50
150
Migration distance (μm)
G
Down
Stable
Up
−log10 (padj)
log2(fold change)
Mmp1
sas
scb
Dg
dally
dlp
Dl
crb
Ras85D
tkv
Hop
Egfr
Tollo
Vamp7
dome
btl
Arpc1
ft
Stam
H
membrane organization
cell-cell adhesion
transmembrane receptor protein tyrosine kinase signaling pathway
regulation of vesicle-mediated transport
vesicle organization
membrane fusion
receptor signaling pathway via JAK-STAT
receptor-mediated endocytosis
0.02
0.04
0.06
GeneRatio
p-value
0.006
0.004
0.002
Count
10
15
20
25
30
35
I
Unoccupied
Occupied
Upd2
Domeless
FKBP12
cpYFP OFF
cpYFP ON
J
DIPF

Figure 3

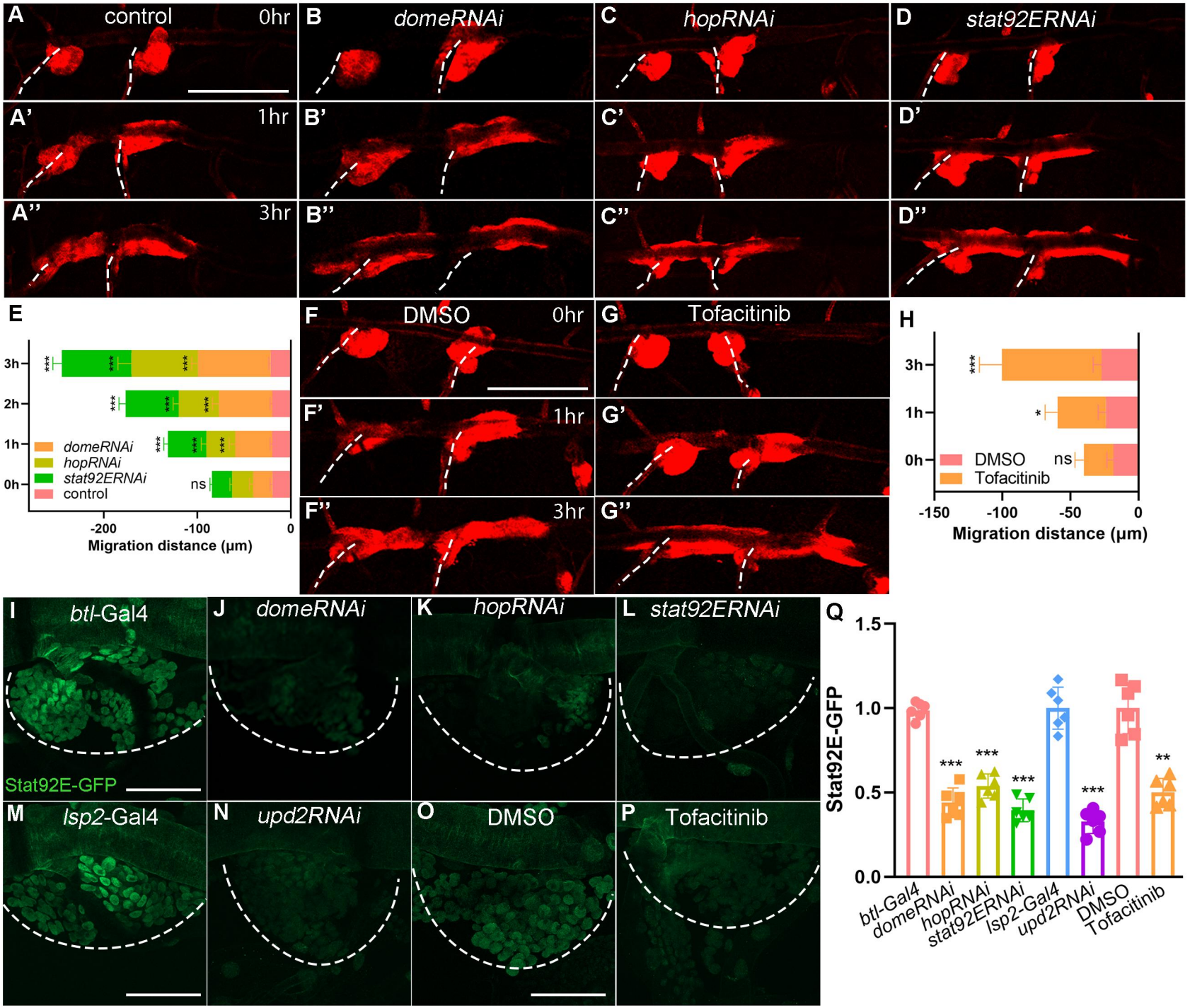
A control 0hr
B domeRNAi
C hopRNAi
D stat92ERNAi
A' 1hr
B'
C'
D'
A'' 3hr
B''
C''
D''
E
3h
2h
1h
0h
domeRNAi
hopRNAi
stat92ERNAi
control
ns
-200
-100
0
Migration distance (μm)
F DMSO 0hr
G Tofacitinib
F' 1hr
G'
F'' 3hr
G''
H
3h
1h
0h
DMSO
Tofacitinib
ns
-150
-100
-50
0
Migration distance (μm)
I btl-Gal4
J domeRNAi
K hopRNAi
L stat92ERNAi
Stat92E-GFP
M lsp2-Gal4
N upd2RNAi
O DMSO
P Tofacitinib
Q
Stat92E-GFP
1.5
1.0
0.5
0.0
btl-Gal4
domeRNAi
hopRNAi
stat92ERNAi
lsp2-Gal4
upd2RNAi
DMSO
Tofacitinib

Figure 4

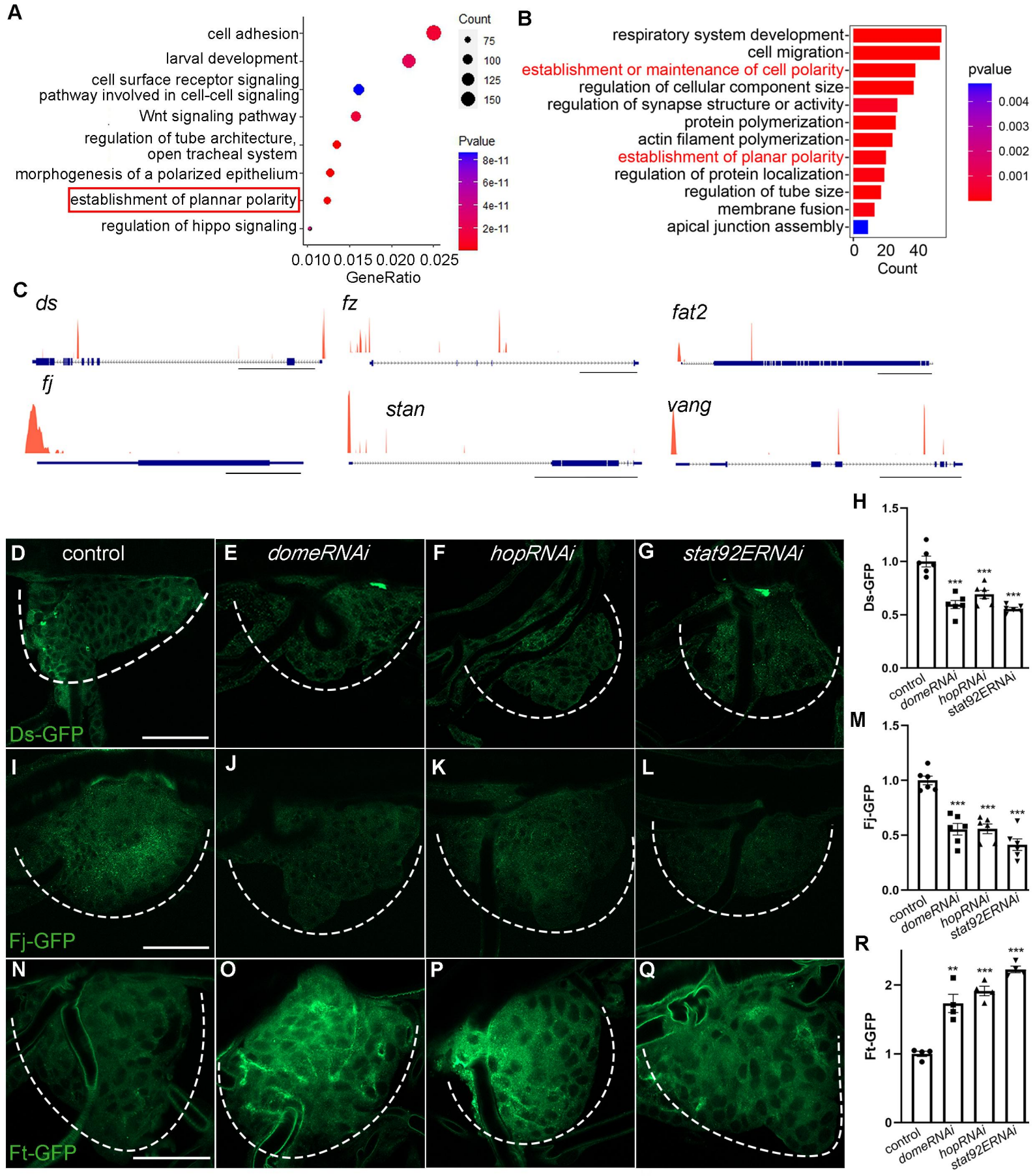
A
cell adhesion
larval development
cell surface receptor signaling pathway involved in cell-cell signaling
Wnt signaling pathway
regulation of tube architecture, open tracheal system
morphogenesis of a polarized epithelium
establishment of plannar polarity
regulation of hippo signaling
0.010 0.015 0.020 0.025
GeneRatio
Count
75
100
125
150
Pvalue
8e-11
6e-11
4e-11
2e-11
B
respiratory system development
cell migration
establishment or maintenance of cell polarity
regulation of cellular component size
regulation of synapse structure or activity
protein polymerization
actin filament polymerization
establishment of planar polarity
regulation of protein localization
regulation of tube size
membrane fusion
apical junction assembly
0 20 40
Count
pvalue
0.004
0.003
0.002
0.001
C
ds
fz
fat2
fj
stan
vang
D control
E domeRNAi
F hopRNAi
G stat92ERNAi
Ds-GFP
I
J
K
L
Fj-GFP
N
O
P
Q
Ft-GFP
H
Ds-GFP
control
domeRNAi
hopRNAi
stat92ERNAi
M
Fj-GFP
R
Ft-GFP

Figure 5

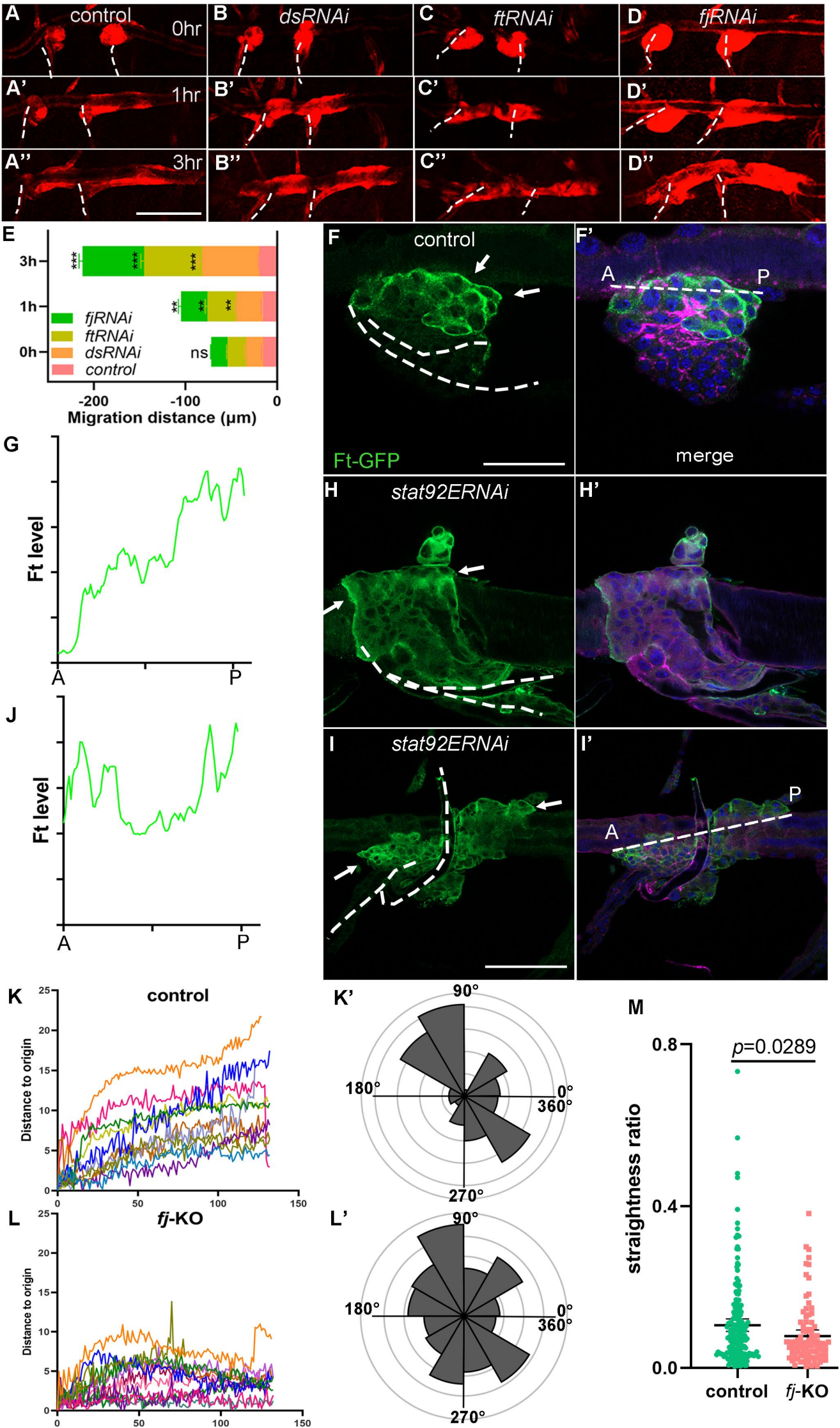
A
control
0hr
B
dsRNAi
C
ftRNAi
D
fjRNAi
A'
1hr
B'
C'
D'
A''
3hr
B''
C''
D''
E
3h
1h
0h
fjRNAi
ftRNAi
dsRNAi
control
***
**
ns
-200
-100
0
Migration distance (μm)
F
control
Ft-GFP
F'
A
P
merge
G
Ft level
A
P
H
stat92ERNAi
H'
I
stat92ERNAi
I'
J
Ft level
A
P
K
control
Distance to origin
K'
90°
180°
0°
360°
270°
L
fj-KO
Distance to origin
L'
90°
180°
0°
360°
270°
M
p=0.0289
straightness ratio
0.8
0.4
0.0
control
fj-KO

Figure 6

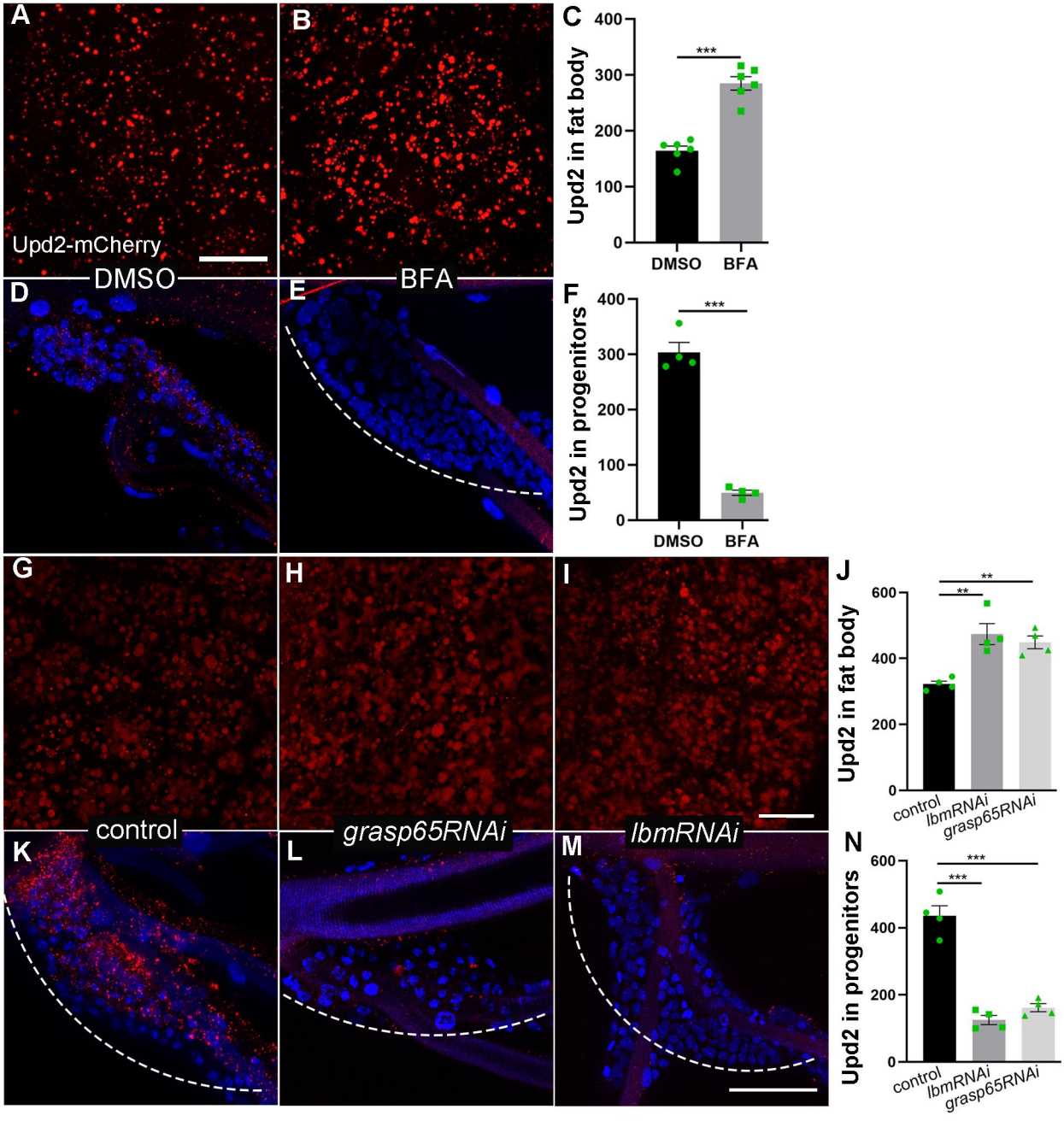
A
B
Upd2-mCherry
DMSO
BFA
C
Upd2 in fat body
400
300
200
100
0
***
DMSO
BFA
D
E
F
Upd2 in progenitors
400
300
200
100
0
***
DMSO
BFA
G
H
I
control
grasp65RNAi
lbmRNAi
J
Upd2 in fat body
600
400
200
0
**
**
control
lbmRNAi
grasp65RNAi
K
L
M
N
Upd2 in progenitors
600
400
200
0
***
***
control
lbmRNAi
grasp65RNAi

Figure 7

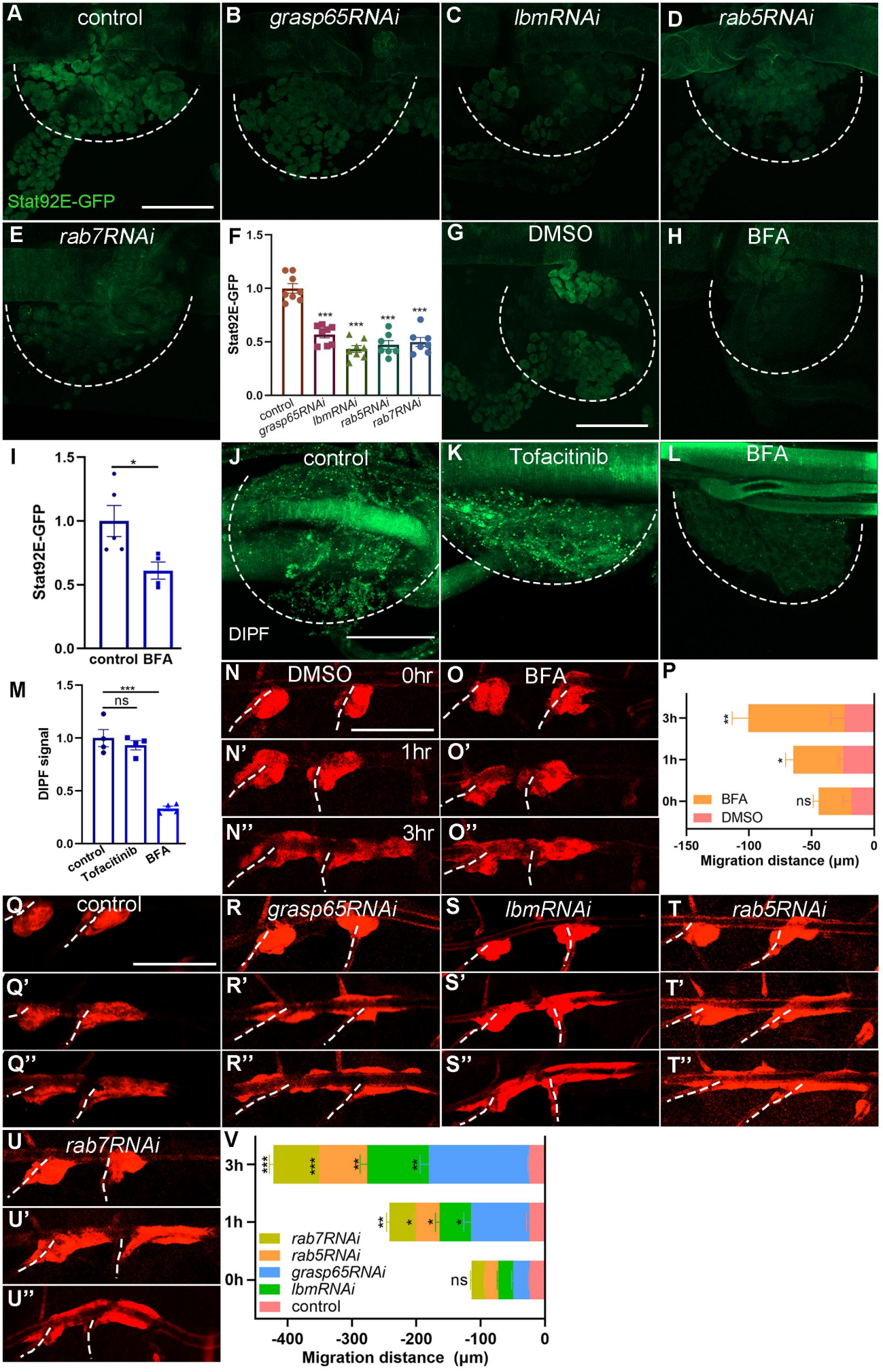
A control
Stat92E-GFP
B grasp65RNAi
C lbmRNAi
D rab5RNAi
E rab7RNAi
F
Stat92E-GFP
control
grasp65RNAi
lbmRNAi
rab5RNAi
rab7RNAi
G DMSO
H BFA
I
Stat92E-GFP
control BFA
J control
DIPF
K Tofacitinib
L BFA
M
DIPF signal
control
Tofacitinib
BFA
ns
N DMSO 0hr
N' 1hr
N'' 3hr
O BFA
O'
O''
P
3h
1h
0h
BFA
DMSO
ns
Migration distance (μm)
Q control
Q'
Q''
R grasp65RNAi
R'
R''
S lbmRNAi
S'
S''
T rab5RNAi
T'
T''
U rab7RNAi
U'
U''
V
3h
1h
0h
rab7RNAi
rab5RNAi
grasp65RNAi
lbmRNAi
control
ns
Migration distance (μm)

Figure 8

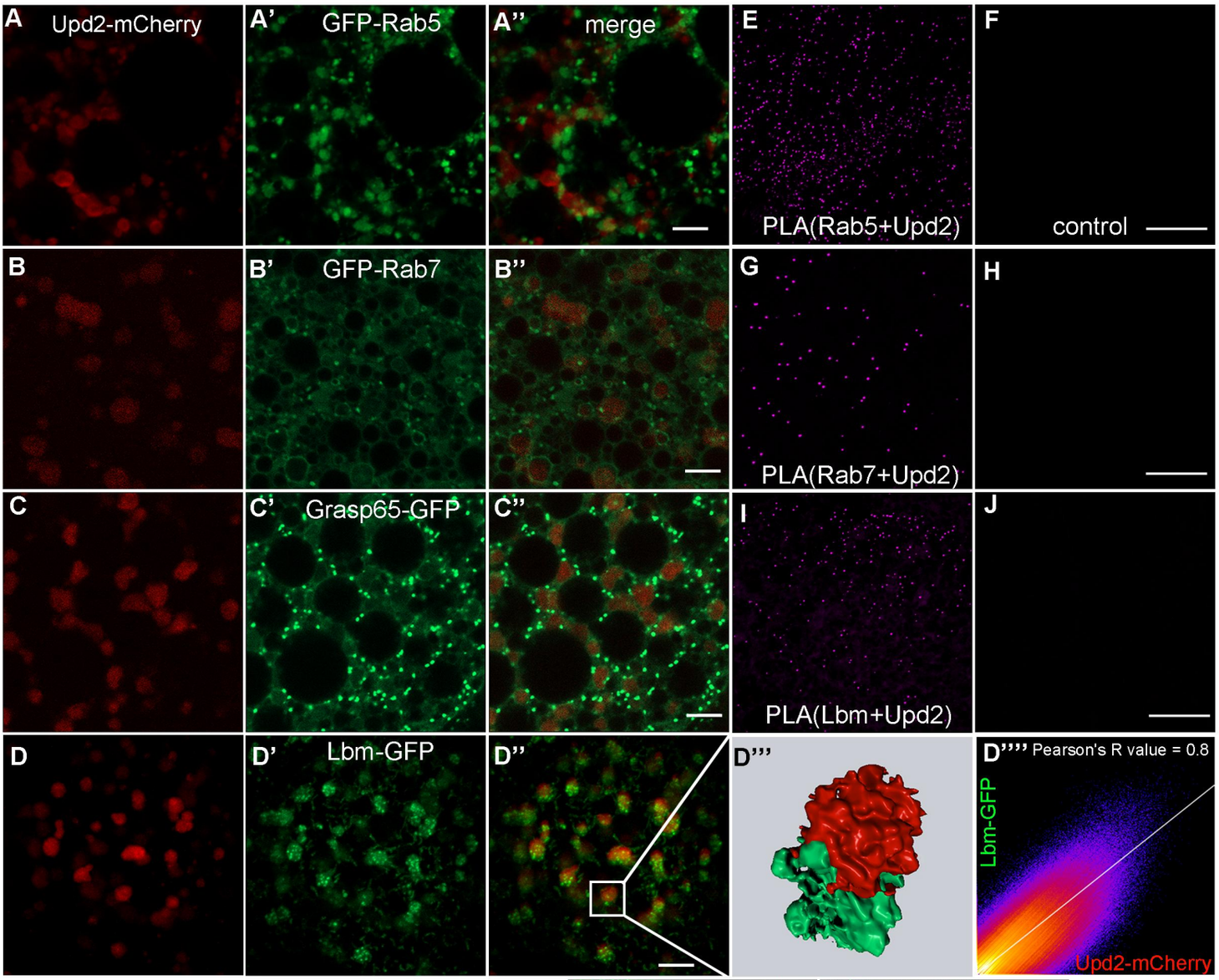
A
Upd2-mCherry
A'
GFP-Rab5
A''
merge
E
PLA(Rab5+Upd2)
F
control
B
B'
GFP-Rab7
B''
G
PLA(Rab7+Upd2)
H
C
C'
Grasp65-GFP
C''
I
PLA(Lbm+Upd2)
J
D
D'
Lbm-GFP
D''
D'''
D'''' Pearson's R value = 0.8
Lbm-GFP
Upd2-mCherry

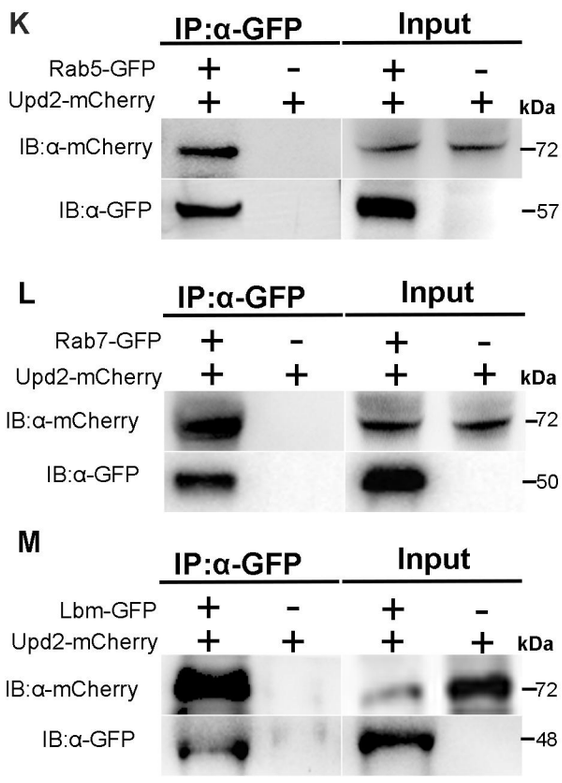
K
IP:α-GFP
Input
Rab5-GFP + - + -
Upd2-mCherry + + + +
kDa
IB:α-mCherry
IB:α-GFP
72
57
L
IP:α-GFP
Input
Rab7-GFP + - + -
Upd2-mCherry + + + +
kDa
IB:α-mCherry
IB:α-GFP
72
50
M
IP:α-GFP
Input
Lbm-GFP + - + -
Upd2-mCherry + + + +
kDa
IB:α-mCherry
IB:α-GFP
72
48

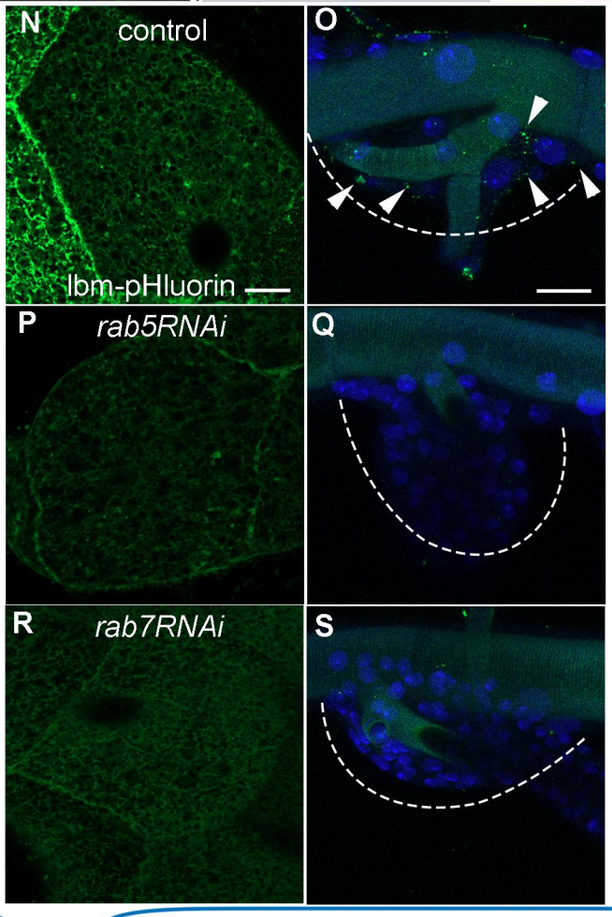
N
control
lbm-pHluorin
O
P
rab5RNAi
Q
R
rab7RNAi
S

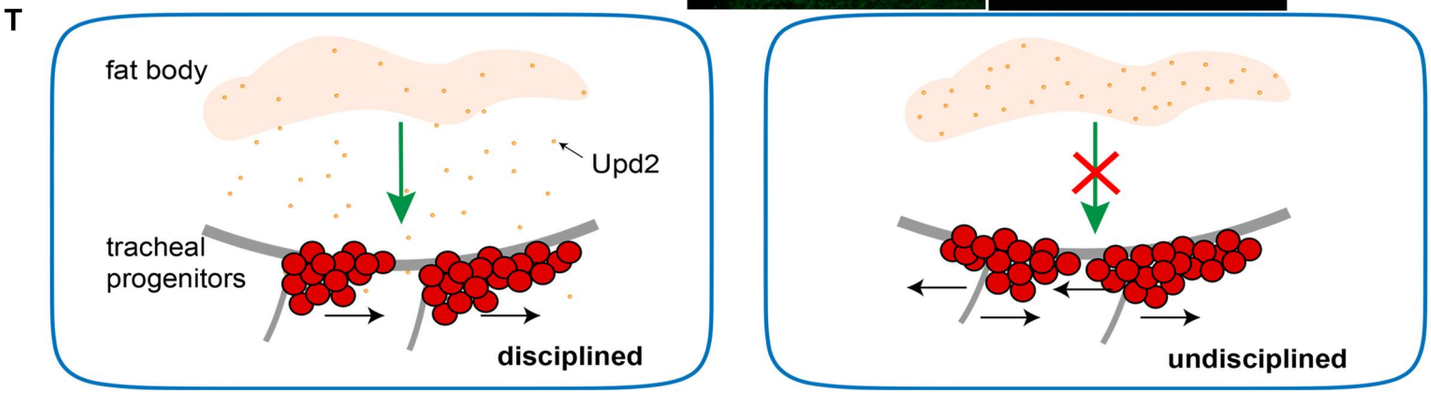
T
fat body
Upd2
tracheal progenitors
disciplined
undisciplined